On the importance of phenology-water interactions in the evaporative process of a semi-arid woodland: Could it be why satellite-based evaporation estimates in the Miombo woodlands differ?

***Henry M. Zimba[1,2], Miriam Coenders-Gerrits[1], Kawawa E. Banda[3], Petra Hulsman[4], Nick van de Giesen[1], Imasiku A. Nyambe[3], Hubert. H. G. Savenije[1].**

[1] Water Resources Section, Faculty of Civil Engineering and Geosciences, Delft University of Technology, Stevinweg 1, 2628 CN Delft, The Netherlands.

[2] Department of Agriculture, Ministry of Agriculture, P.O. Box 50595, Mulungushi House, Independence Avenue, Lusaka, Zambia.

[3] Integrated Water Resources Management Centre, Department of Geology, School of Mines, University of Zambia, Great East Road Campus, Lusaka, Zambia.

[4] Ghent University, Hydro-Climate Extremes Lab (H-CEL), Coupure links 653, 9000 Ghent, Belgium

*****Corresponding author: a.m.j.coenders@tudelft.nl

Abstract

The miombo woodland is the largest dry woodland formation in sub-Saharan Africa with a spatial extent approximated between 2.7 – 3.6 million km^2. In comparison to other global ecosystems the miombo woodland exhibits unique ecohydrological properties such as increase in the leaf area index (LAI) in the dry season. However, due to limited flux observations in the miombo region, there is scarcity of information on the effect of these properties on evaporation of the miombo woodland. Better understanding of evaporation of the miombo is required for accurate hydrological and climate modelling of this region. The only regional evaporation estimates available are from satellite-based products. However, due to the scarcity of information, there is doubt about their accuracy. Therefore, in this study trends and magnitudes of six satellite-based evaporation estimates (FLEX-Topo, GLEAM, MOD16, SSEBop, TerraClimate and WaPOR) are compared over the different seasons in the miombo woodland of the Luangwa Basin, a representative river basin in southern Africa. In this comparison we check if the trends and magnitudes of the satellite-based evaporation estimates align with the documented phenology-water interactions of the miombo woodland. In the absence of basin scale field observations, actual evaporation estimates based on the multi-annual water balance (E_{wb}) are used for comparison.

Results show that satellite-based evaporation estimates differ substantially from each other within the different seasons, i.e., the cool-dry season, warm dry season and warm-pre-rainy season. The latter is a characteristic season when the miombo species undergo substantial changes in the canopy phenology, whereby leaf-fall and leaf-flush occur at the same time, and there is access to deeper moisture stocks to support leaf-flush in preparation of the rainy season. During the warm dry season, the satellite-based evaporation estimates differ most from each other, while the best agreement is reached during the periods with high temperature, high soil moisture, high leaf chlorophyll content and highest LAI (i.e., rainy season). Compared to the basin-scale actual evaporation, all six satellite-based evaporation estimates appear to underestimate evaporation. Overall, it appears that inadequate understanding and inaccurate representation of the phenology-

water interactions of the miombo species are the cause of these discrepancies. Based on this study, field-based observations of the evaporation during the different seasons are required to enhance satellite-based evaporation estimates in the miombo woodlands.

1 Introduction

Vegetation phenology refers to the periodic biological life cycle events of plants, such as leaf-flushing, senescence and corresponding temporal changes in vegetation canopy cover (Stökli *et al.*, 2011; Cleland *et al.*, 2007). Plant phenology and climate are highly correlated (Pereira *et al.*, 2022; Niu *et al.*, 2013; Cleland *et al.*, 2007). Plants respond to triggers, such as temperature, hydrology and day light, by initiating among others: leaf-fall, leaf-flush, budburst, flowering and variation in photosynthetic activity (Pereira *et al.*, 2022; Niu *et al.*, 2013; Cleland *et al.*, 2007). Phenological responses are species-dependent and are controlled by adapted physiological properties (i.e., Lu *et al*., 2006). Plant phenology controls the access to critical soil resources such as nutrients and water (Nord and Lynch, 2009). Moreover, phenological response influences plant canopy cover and affects plant-water interactions. Variations in canopy leaf display, i.e., due to leaf-fall and leaf-flush, influences how much radiation is intercepted by plants (Shahidan, Salleh, and Mustafa, 2007). Intercepted radiation influences canopy conductance. In water limited conditions, at both individual species and woodland scales, leaf-fall reduces canopy radiation interception while leaf-flush and the consequent increase in canopy cover increases canopy radiation interception leading to increased transpiration (Snyder and Spano, 2013), controlled by moisture availability, whether in the vegetation itself or in the root zone. Plant canopy cover and its interactions with atmospheric carbon dioxide influences transpiration. Ultimately, plant phenological response to changes in the triggers influences transpiration and actual evaporation of the woodland (i.e., Marchesini *et al.*, 2015).

Evaporation of woodland surfaces accounts for a significant portion of the water cycle over the terrestrial landmass (Sheil, 2018; Van Der Ent *et al*., 2014; Gerrits, 2010; Van Der Ent *et al*., 2010). Miralles *et al.* (2020) defined evaporation as "the phenomenon by which a substance is converted from its liquid into its vapour phase, independently of where it lies in nature". In this study we adopt the term evaporation for all forms of terrestrial evaporation, including transpiration by leaves, evaporation from intercepted rainfall by vegetation and woodland floor, soil evaporation, and evaporation from stagnant open water and pools (Savenije, 2004). Understanding the characteristics of evaporation, such as interception and transpiration, in various woodland ecosystems is key to monitoring the climate impact on woodland ecosystems and for hydrological modelling and the management of water resources at various scales (Kleine *et al.*, 2021; Bonnesoeur *et al.*, 2019; Roberts, (undated)). Knowledge of the woodland phenology interactions with climate variables and seasonal environmental regimes is key to this understanding (i.e., Zhao *et al.*, 2013). Environmental variables such as precipitation and temperature influences plant phenology differently across the diverse ecosystems globally (Forrest *et al.*, 2010; Forrest & Miller-Rushing, 2010; Kramer *et al.*, 2000). Additionally, Tian *et al.* (2018) showed that, at the ecosystem scale, plants have adapted to local climatic (such as precipitation, temperature, and radiation) and abiotic (such as soil type and soil water supply) conditions. The findings by Tian *et al.* (2018) are "evidence of global differences in the interaction between plant water storage and leaf phenology". Although this study referred to within-plant storage of moisture it may be as relevant to root zone storage or access to groundwater. Therefore, understanding the plant

phenology-water interactions at local and regional scales and appropriately incorporating these aspects in hydrological and climate modelling is likely to improve accuracy of the simulations (i.e., Forster *et al*., 2022).

The miombo woodlands is the largest dry woodland formation in sub-Sahara Africa with a spatial extent approximated between 2.7 – 3.6 million km^2, covering about 10% of the continent (Ryan *et al.*, 2016; Frost, 1996; White, 1983). Despite their significance for biodiversity (Mittermeier *et al.*, 2003, White, 1983), carbon sink (Pelletier *et al.*, 2018) and the food, energy and water nexus (Beilfuss, 2012; Campbell *et al.*, 1996; Frost, 1996), little attention has been paid to its hydrological functioning. The uniqueness of its plant-water interactions has been highlighted (Tian *et al.*, 2018; Guan *et al.*, 2014; White, 1983) and has been particularly demonstrated by Tian *et al.* (2018), Vinya *et al.*, (2018), Fuller (1999), Frost (1996) and White (1983). Of particular importance is its control of leaf phenology (i.e., Vinya *et al.*, 2018), co-occurring of leaf-fall (leaf shedding) and leaf-flush (i.e., Fuller, 1999), and deep rooting, which allows miombo species to access deep soil moisture, including groundwater, to buffer for dry season water limitations (Tian *et al.*, 2018; Guan *et al.*, 2014, Savory, 1963). Most remarkably, new leaf-flushing occurs before the commencement of seasonal rainfall (Chidumayo, 1994; Fuller and Prince, 1996). Young flushed leaves in the dry season have high water content of up to 66% which declines to about 51% as the leaves harden, until they are shed off in the next season (Ernst and Walker, 1973). The miombo woodland is heterogeneous with diverse plant species whose phenological response to stimuli is species-dependent (Chidumayo, 2001; Fuller, 1999; Frost, 1996). For instance, leaf-fall, leaf-flush and leaf colour change are triggered at different times for each species. This means that the miombo woodland is unlike other woodlands where leaf-fall and leaf-flush occur in different seasons. In the Miombo, co-occurring of leaf-fall and leaf-flush results in a woodland canopy that is variable in terms of canopy closure and greenness especially during the dry season. As a result, it has varied canopy closure ranging from 2 to about 70 percent depending on the miombo woodland strata and local environmental conditions such as rainfall, soil type, soil moisture, species composition and temperature (Chidumayo, 2001; Fuller, 1999; Frost, 1996). For the wet miombo woodland with a canopy closure of about 70 percent, at any given time, there is a relatively large woodland canopy surface for radiation interception. The deep rooting in most miombo species (Savory, 1963) provides access to deep soil moisture resources (Fan *et al.*, 2017; Kleidon and Heimann, 1998). As a result, the canopy provides an evaporative surface that, in combination with other environmental variables, possibly facilitates continued transpiration even during the driest periods (i.e., Li *et al.*, 2021). Most miombo species are broad leaved with capacity for radiation interception (Fuller, 1999) and rainfall interception of up to 20% in wet miombo woodland (Alexandre, 1977). It appears that in the miombo woodland soil moisture increases with depth (Chidumayo, 1994; Jeffers and Boaler, 1996; Savory, 1963). These typical phenological and physiological attributes are of particular importance for evaporative processes (Forster *et al*., 2022; Snyder *et al*., 2013; Schwartz, 2013).

Regardless of the uniqueness and importance of the miombo woodland, there exists scant, if any, information on its evaporation dynamics. Most of studies in the miombo woodland concentrated on the characterisation of woodland plant species, its role as a carbon sink and the social-economic relevance of the ecosystem. There is ample information on the phenology of plant species (e.g.: Chidumayo *et al.*, 2010; Chidumayo, 2001; Fuller, 1999; Chidumayo and Frost, 1996), but there have been very limited attempts to characterise evaporation of the ecosystem, especially during the dry season. The only point-based field observations of evaporation of the wet

miombo woodland by Zimba *et al.* (2013) are not sufficient to make any definitive conclusions about the evaporative dynamics of this vast ecosystem.

In the absence of spatially distributed field observations, satellite-based evaporation estimates are valuable alternatives, though they come with their own limitations (Zhang *et al.*, 2016). It is well-realised that evaporation depends on land cover (Han et *al.*, 2019; Liu & Hu, 2019; Wang *et al.*, 2012), but, because of the differences in algorithms, process and inputs, satellite-based evaporation estimates differ for the same land surface (Zhang *et al.*, 2016; Cheng *et al.*, 2014). Currently, satellite-based evaporation estimates at various scales are available (e.g.: Global land evaporation Amsterdam model (GLEAM) (Martens et al., 2017; Miralles et al., 2011); Moderate-resolution imaging spectrometer (MODIS) MOD16) (Running et al., 2019; Mu et al., 2011; Mu et al., 2007); Operational simplified surface energy balance (SSEBop) (Senay et al., 2013); and Water productivity through open access of remotely sensed derived data (WaPOR) (FAO, 2018)). Classification of the various satellite-based evaporation estimates have been extensively discussed by Zhang *et al.* (2016), Jiménez *et al.* (2011) and Jiménez, Prigent & Aires (2009). These satellite-based evaporation estimates have mainly been designed for agricultural crops (i.e., Biggs *et al.*, 2015; Zhang *et al.*, 2016). However, natural woodlands have different phenology-water interactions and evaporation characteristics (Wang-Erlandsson *et al.*, 2016; Snyder and Spano, 2013; Schwartz, 2013). There is currently no publication in the public domain showing how various satellite-based evaporation estimates compare in the miombo woodland, especially with a focus on the unique interactions between phenology and hydrology in miombo species across different phenophases and seasons. Yet, the use of satellite-based evaporation estimates in hydrological modelling, climate modelling and the management of water resources, globally and in Africa, is increasing (i.e., García *et al.*, 2016; Zhang *et al., 2016;* Makapela, 2015). However, because of the absence or scarce field observations and extremely limited validation, it is impossible to know which satellite-based evaporation estimates are close to the actual conditions of the miombo woodland. If any, the choice for a satellite-based evaporation product is based on validation results in non-miombo woodlands or at a scale (i.e., Weerasinghe *et al.*, 2020) that includes other woodland types. Obviously, an evaporation estimation approach that performs well in energy limited conditions or homogeneous woodlands (i.e., Bogawski and Bednorz, 2014) cannot be assumed to have the same performance in a warm, water limiting and heterogeneous woodland such as the miombo. Although, Weerasinghe *et al.* (2020) compared satellite-based evaporation estimates in the Zambezi Basin, whose vegetation cover, among many others, comprises the miombo woodland, the focus of their study was not on the miombo woodland. Furthermore, Weerasinghe *et al.* (2020) did not attempt to link the differences in the satellite-based evaporation estimates to the phenology of the miombo woodland. The results they observed at the Zambezi Basin scale might be different at sub-basin level such as the Luangwa Basin.

This study addresses the performance of satellite-based evaporation estimates during different phenophases of the miombo woodland with a focus on the Luangwa sub-basin of the Zambezi, one of the largest river basins in the miombo ecosystem. The Luangwa basin contains both dry (i.e., southern miombo woodlands) and wet (i.e., central Zambezian miombo woodlands) miombo. The central Zambezian miombo woodland is the largest of the four miombo woodland sub-groups, the other three being the Angolan miombo woodland, eastern miombo woodland, and the southern miombo woodland (Frost, 1996; White, 1983). The Luangwa Basin is largely covered by miombo woodland with the mopane woodland occupying a much smaller area of the basin (Frost, 1996; White, 1983). These attributes suggest a catchment that provides a fair representation of miombo woodlands and an appropriate site for studying its evaporation characteristics.

Hence, the aim of this study is two-fold:

(i) Compare the temporal trends and magnitudes of six freely available satellite-based evaporation products across different phenophases of the miombo woodland.

(ii) Compare satellite-based evaporation estimates to the water balance-based actual evaporation estimates for the Luangwa Basin.

2 Materials and Methods

2.1 Study site

The location and extent of the miombo woodland in Africa is presented in Fig. 1(a) (Ryan *et al.*, 2016; White, 1983). The Luangwa (Fig. 1b) is a sub-basin of the Zambezi Basin in sub-Saharan Africa in Zambia with spatial extent of about 159,000 km^2 (Beilfuss, 2012; World Bank, 2010). Based on the miombo woodland delineation by White (1983) and Ryan *et al.* (2016) as given in Fig.1 (c) about 75 percent of the total Luangwa Basin land-mass is covered by the miombo woodland, both dry and wet miombo.

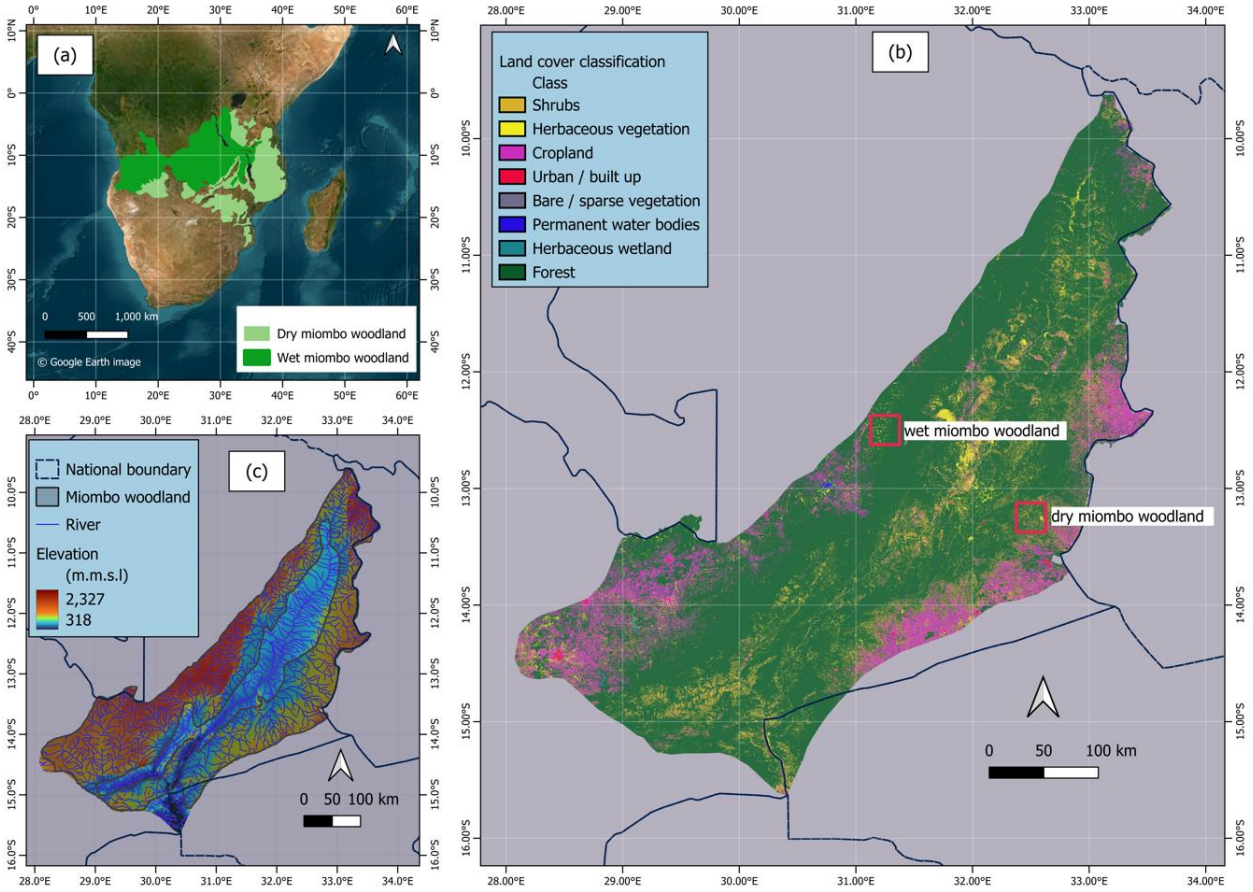

Figure 1: (a) Spatial extent of the miombo woodland in Africa and the location of the Luangwa Basin in Zambia. (b) Spatial distribution of elevation ASTER digital elevation model (DEM) and the extent of the miombo woodland in the Luangwa Basin. (c) Land cover characterisation of the Luangwa Basin based on the Copernicus land cover classification.

Additionally, statistics from the 2019 Copernicus land cover classification (Fig. A1 in the supplementary data), indicates that 77 % of the total basin area is woodland (dense and open woodland) which is largely miombo woodland with a smaller component of mopane woodland in the middle area of the basin (Buchhorn *et al.*, 2020; Martins *et al.*, 2020). Elevation (Fig. 1b) ranges between 329 – 2210 m with the central part generally a valley. The miombo woodland, both dry and wet miombo, is generally in the upland (Fig.1b). The Luangwa River, 770 km long, drains the basin and is scarcely gauged (Beilfuss, 2012). This has resulted in a paucity of data on various hydrological aspects such as rainfall and discharge. The climate is characterised by a well-delineated wet season, from October to April, and a dry season, from May to October. Furthermore, the dry season is split into the cool-dry (May to August) and hot dry (August to October) seasons. The movement of the inter-tropical convergence zone (ITCZ) over Zambia between October and April dominates the rainfall activity in the basin. The basin has a mean annual precipitation of about 970 mm yr^{-1}, potential evaporation of about 1560 mm yr^{-1}, and river runoff reaches about 100 mm yr^{-1} (Beilfuss, 2012; World Bank, 2010). The key character of the miombo woodland species is that it sheds off old leaves and acquires new ones during the period May to October during the dry season. Depending on the amount of rainfall received in the preceding rain season the leaf-fall and leaf-flush processes may start early (i.e., in case of low rainfall received) or late (in case of high rainfall received) and may continue up to November (i.e., in the case of high rainfall received) (Frost,1996).

2.2 Study approach

The study sought to find out the extent to which satellite-based evaporation estimates agree with each other during the different canopy phenophases of the miombo woodland. Point scale observations in the wet miombo woodland (Zimba *et al.*, 2023) showed that satellite-based evaporation estimates underestimated actual evaporation of the wet miombo woodland during the dry season and early rainy season in the Luangwa Basin. However, the Luangwa Basin has a heterogenous land cover which includes mopane woodland and grasslands. The question was whether the heterogeneity in the land cover of the Luangwa Basin would result in satellite-based evaporation estimates performing contrary to the point-scale observations at a wet miombo woodland site when compared to the water balance-based evaporation estimates at basin scale.

For this study, a 12-year period, 2009–2020, was used because satellite-based evaporation estimates were available for free for this period. The period also had cycles of low and high annual rainfall allowing to analyse performance under changing monthly and annual conditions. The following sections elaborate the methods used in this study.

2.2.1 Phenophases of the miombo woodland and assessment of phenological conditions

To categorise the phenophases two approaches were used: satellite-based classification and climate and soil moisture-based classifications.

Satellite-based classification of phenophases has been based on the National Aeronautics and Space Administration (NASA) Collection 6 MODIS Land Cover Dynamics (MCD12Q2) Product accessed from the https://modis.ornl.gov/globalsubset/, last access: 20 February, 2023 (Gray *et al.*, 2019; Friedl et *al.,* 2019; Zhang *et al.,* 2003). The MCD12Q2 uses the changes in canopy greenness to characterise the canopy phenophases (Friedl et *al.,* 2019; Gray *et al.,* 2019). For the miombo woodland in the Luangwa Basin eight phenophases were identified using the satellite-based data MCD12Q2 (Fig. 2). The satellite-based phenophases include: green-up, mid-green up, maturity, peak, senescence, green-down, and mid-green down and dormant. For easy of

analysis the phenophases were merged into four groups based on dominant activity in each phenophase (Fig. 2). To compliment the MCD12Q2 classification the MODIS-based leaf area index (LAI) obtained from https://modis.ornl.gov/globalsubset/, last access: 20 February, 2023) (Myneni, Knyazikhin & Park, 2021; ORNL DAAC, 2018; Myneni & Park, 2015) and the normalised difference vegetation index (NDVI) (ORNL DAAC, 2018; Vermote and Wolfe, 2015) were used.

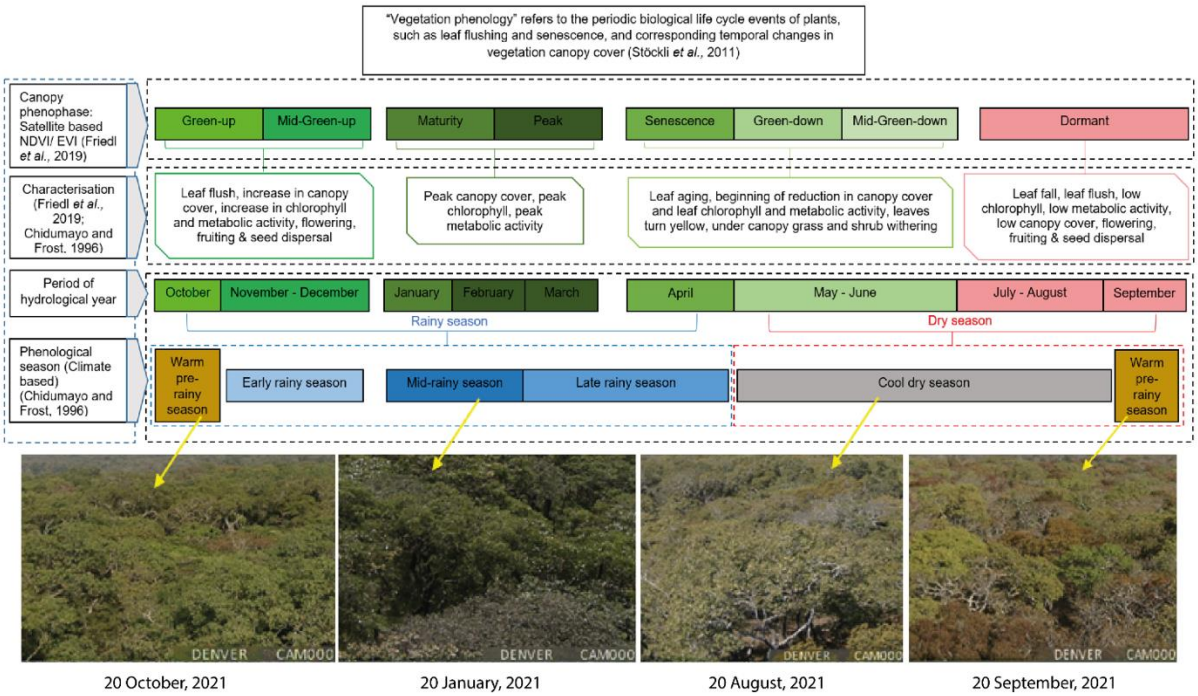

Figure 2: Characterisation of canopy phenophases of the miombo woodland in relation to seasonality for the Luangwa Basin. Photographs show the changes in the canopy cover on selected days across different phenophases of a wet miombo woodland for the year 2021.

The satellite-based LAI and NDVI have been used before as proxies to observe phenological conditions such as the canopy biomass formation, changes in the canopy closure (i.e., through leaf-fall and leaf-flush) and changes in canopy chlorophyll conditions (i.e., Guan *et al.*, 2014; Santin-Janin *et al.*, 2009; Chidumayo, 2001; Fuller, 1999). For the LAI the NASA's MCD15A3H product (Myneni, Knyazikhin & Park, 2021; ORNL DAAC, 2018; Myneni & Park, 2015) with a four-day temporal resolution and 500 m spatial resolution has been used. The MODIS MOD09GQ.006 (Vermote and Wolfe, 2015) surface reflectance bands 1,5 and 6 have been used to estimate the NDVI at daily temporal resolution and 250 m spatial resolution using the band ratio method. The daily NDVI values were then averaged into four-day values to obtain the same temporal resolution as the LAI.

For the climate and soil moisture-based classification Chidumayo and Frost (1996) observed five phenological seasons: warm pre-rainy season, early rainy season, mid-rainy season, late rainy season and the cool dry season (Fig. 2). For easy of analysis, the above three rainy season phenophases were merged into one rainy season phenophase. Therefore, three climate and soil moisture-based phenophases were established; warm pre-rainy season, rainy season and the cool dry season. Within these phenological seasons the phenology of miombo species transitions through various stages i.e., from leaf-fall/leaf-flush, growth of stems, flowering to mortality of

seed (Chidumayo and Frost,1996).

To compliment the observations, photographs from a digital camera (Denver WCT-8010) installed on the flux tower at a wet miombo woodland site in Mpika (Zimba *et al.,* 2023) were used to observe the changes in the canopy phenology of the miombo woodland across different phenophases from January to December in the year 2021. In addition, the fish-eye (LIEQI LQ-001) was used to obtain canopy images. The images of the canopy helped to observe the changes and differences in canopy leaf display (i.e., leaf-fall, leaf-flush and leaf colour changes) among miombo species.

2.2.2 Delineation of the miombo woodland areas used in this study

The comparison of satellite-based evaporation estimates was performed at two levels: using a grid at a known dry miombo woodland and wet miombo woodland locations, and at the entire miombo woodland scale in the Luangwa Basin (Figs. 1 and 3).

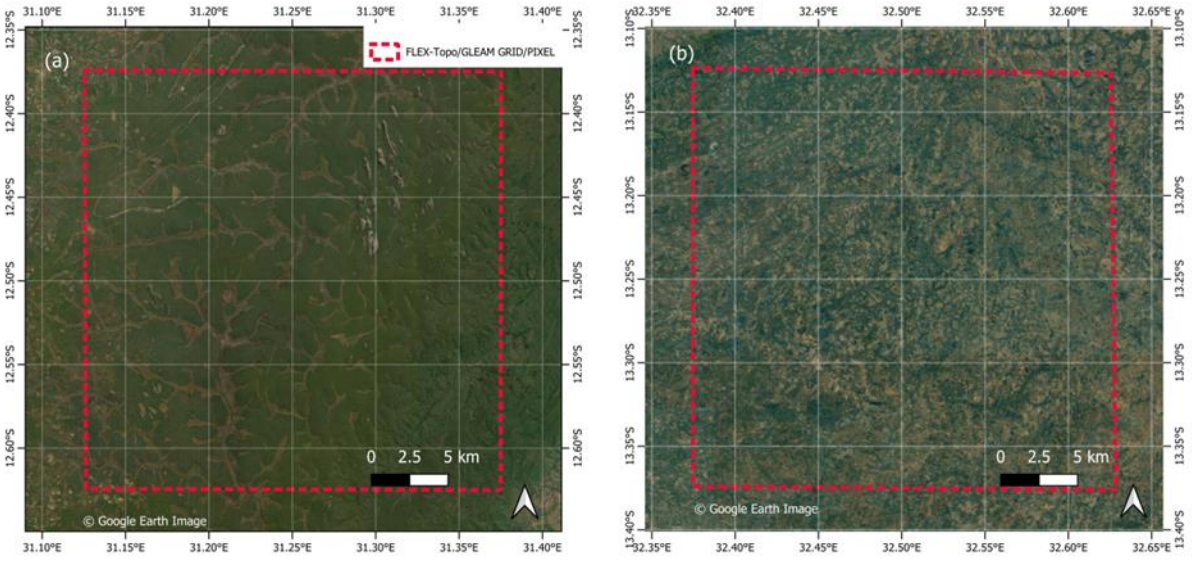

Figure 3: The wet miombo woodland (a) and dry miombo woodland (b) locations used for comparison of satellite-based evaporation estimates at FLEX-Topo and GLEAM spatial resolution (approximately 27.7 km by 27.7 km). The dotted red line is the actual location of the FLEX-Topo and GLEAM pixels.

Firstly, a comparison based on the 27.7km by 27.7km grid was performed by using known undisturbed wet miombo woodland and dry miombo woodland locations (Figs. 1 and 3). The grid was based on the satellite-based evaporation estimates (i.e., FLEX-Topo and GLEAM) with the largest spatial resolutions (approximately 27.7 km by 27.7 km) (Fig. 3 and Table 1). For MOD16, SSEBop, TerraClimate and WaPOR, the mean of actual evaporation estimates in all the pixels within the dotted red square (Fig. 3) were used. The focus on a known wet miombo woodland enabled comparison of the field observations of the changes in canopy cover using digital camera images to the satellite-based LAI and NDVI for the year 2021. See Section 2.2.3 and Table 1 for satellite-based evaporation estimates used in this study.

Secondly, the typical miombo woodland regions as categorised by White (1983) and Ryan

et al. (2016) (see Fig. 1 a,b) were used to delineate the area covered by the miombo woodland in the Luangwa Basin. The delineated miombo woodland in the Luangwa Basin excluded the mopane woodland, mixed woodland as well as the water bodies. This delineation (as shown in Fig. 1) ensured that only the areas classified as typical miombo woodland (Ryan *et al.*, 2016; White, 1983) were considered in the analysis.

2.2.3 Satellite-based products used in the study

The six satellite-based evaporation estimates consisted of: 1) FLEX-Topo (Hulsman *et al.*, 2021; Hulsman *et al.*, 2020; Savenije, 2010); 2) Thornthwaite-Mather climatic water balance model (TerraClimate) (Abatzoglou *et al.*, 2018); 3) Global land evaporation Amsterdam model (GLEAM) (Martens *et al.*, 2017; Miralles *et al.*, 2011); 4) Moderate-resolution imaging spectrometer (MODIS) MOD16 (Running *et al.*, 2019; Mu *et al.*, 2011; Mu *et al.*, 2007); 5) Operational simplified surface energy balance (SSEBop) (Senay *et al.*, 2013) and 6) Water productivity through open access of remotely sensed derived data (WaPOR) (FAO, 2018). These satellite-based evaporation estimates were selected purely because they are free of charge and easily accessible from various platforms and have an archive of historical data with the temporal and spatial resolutions suitable for use in this study. Except for FLEX-Topo and GLEAM (with spatial resolution of 27.7 km), these satellite-based evaporation estimates have relatively fine spatial resolution (i.e., 500 m, 1000 m, 4000 m and 250 m for MOD16, SSEBop, TerraClimate and WaPOR respectively) and temporal resolution (daily, 8-day, 10-day and monthly respectively), which attributes were suitable for this study. The original spatial resolutions were used because these satellite-based evaporation estimates are normally used as is, in their original resolutions. Resampling the different spatial resolutions of the satellite-based evaporation estimates to a single (uniform) spatial resolution was thought to be problematic as it would have introduced unknown and unquantifiable errors, regardless the extent resampled. For detailed explanations on the model structure, processes and inputs for the satellite-based evaporation estimates used in this study the reader is advised to refer to the cited literature above and in Table 1.

Other satellite-based products used in this study include the ASTER digital elevation model (DEM), MODIS-based LAI and NDVI, Copernicus land cover map, net radiation, precipitation, runoff, soil moisture and relative humidity. For detailed information (i.e., structure, processes and inputs) on the other satellite-based products used in this study the reader is advised to refer to the cited literature in Table 1.

2.2.4 Actual evaporation derived from the water balance

In cases where spatially distributed field measurements are not available the water balance approach, using spatially distributed satellite-data, is a practical approach (i.e., Weerasinghe *et al.*, 2020; Liu *et al.*, 2016). In this study the general annual water balance was used to test the performance of the satellite-based evaporation estimates at basin level.

Table 1. Characteristics of products used in the study

Variable	Product name	Time Period	Spatial coverage/Location	Temporal resolution	Spatial resolution	Reference	Source of data
Precipitation	CFSR v2	2009 - 2020	Global	Daily	19.2 km	(Saha *et al.*, 2014; Saha et al., 2010)	Climate Engine portal https://app.climateengine.com/climateEngine
	CHIRPS	2009 - 2020	Global	Daily	4.8 km	(Funk *et al.*, 2015)	Climate Engine portal
	ERA5	2009 - 2020	Global	Daily	24	(Hersbach *et al.*, 2017)	Climate Engine portal
	TerraClimate	2009 - 2020	Global	Monthly	4 km	(Abatzoglou et al., 2018)	Climate Engine portal
Air temperature (mean)	CFSR v2	2009 - 2020	Global	Daily	19.2 km	(Saha *et al.*, 2014; Saha et al., 2010)	Climate Engine portal
LAI	MODIS MCD15A3H v6	2021	Global	4-Day	0.5 km	(Myneni, Knyazikhin & Park, 2015)	Climate Engine portal
NDVI	MODIS MOD09GA v6	2021	Global	Daily	0.5 km	(Vermote & Wolfe, 2015)	Climate Engine portal
Runoff	Observations	1960-1992	159,000 km^2	Daily	N/A		WARMA, Zambia
	TerraClimate	1960 - 2020	Global	Monthly	4 km	(Abatzoglou *et al.*, 2018)	Climate Engine portal
Net radiation	CFSR v2	2009-2020	Global	Daily	19.2 km	(Saha *et al.*, 2014; Saha et al. 2010)	Climate Engine portal
Soil moisture (25 cm)	CFSR v2	2009 -2020	Global	Daily	19.2 km	(Saha *et al.*, 2014; Saha et al. 2010)	Climate Engine portal
Relative humidity	CFSR v2	2009 - 2020	Global	Daily	19.2 km	(Saha *et al.*, 2014; Saha et al. 2010)	Climate Engine portal
Elevation	ASTER GDEM v3	N/A	Global	N/A	30m	(Abrams and Crippen, 2019)	NASA Glovis portal
Land cover map	Copernicus CGLS-LC100 v3	2019	Global	Annual	100m	(Buchhorn *et al.*, 2020)	Google Earth Engine
Actual evaporation	FLEX-Topo	2009 - 2020	Catchment	Daily	27.7 km	(Hulsman *et al.*, 2021; Hulsman *et al.*, 2020; Savenije, 2010)	ZAMSECUR Project – Delft Technical University
	GLEAM (v3.2a)	2009 -2020	Global	Daily	27.7 km	(Martens *et al.*, 2017; Miralles *et al.*, 2011)	GLEAM FTP server
	MOD16v2	2009 -2020	Global	8-Day	0.5 km	(Running *et al.*, 2019; Mu et *al.*, 2011)	Climate Engine portal; Global subsets tool: MODIS/VIIRS Land Products
	SSEBop	2009 -2020	Global	Monthly	1 km	(Senay *et al.*, 2013).	Climate engine portal
	TerraClimate	2009 -2020	Global	Monthly	4 km	(Abatzoglou *et al.*, 2018)	Climate engine portal
	WaPOR v2. (ETLook)	2009 -2020	Continental	10-Day	0.25 km	(FAO, 2018)	WaPOR Portal

The basin average annual water balance-based evaporation ($E_{a_{(wb)}}$) is estimated using Eq. (1) where long-term over-year storage change is disregarded.

$$E_{a_{(wb)}} = P - \mathrm{Q} \quad (1)$$

where, P is the annual average catchment precipitation in mm year^{-1} and Q is annual average discharge in mm year^{-1}. The precipitation and discharge information for the water balance approach were selected and used as explained below.

Ensemble satellite precipitation

The challenge posed by using satellite-based precipitation data in African catchments is that most, if not all, satellite precipitation products are geographically biased towards either underestimation or overestimation, despite some of them having good correlation with ground observations (i.e., Macharia *et al.*, 2022; Asadullah *et al.*, 2008; Dinku *et al.*, 2007). The lack of adequate ground precipitation observations makes it difficult to validate, as well as correct, the product's bias with an acceptable degree of certainty. There is not a single precipitation product that has been found to perform better than other precipitation products across African landscapes and southern Africa in particular (i.e., Macharia *et al.*, 2022). For the Luangwa Basin there is no guarantee that any of the precipitation products are spatially representative of a basin that is about 159,000 km^2 with varying topographical attributes. For instance, compared to point-based field observations of precipitation at six weather stations in Zambia (three stations in the Luangwa Basin and the other three outside of the Luangwa Basin) no single satellite-based precipitation product showed consistency with all weather stations (see Table A1 in the supplementary data). Using an ensemble of precipitation products is said to reduce errors and is therefore recommended (e.g.: Weerasinghe *et al.*, 2020; Asadullah *et al.*, 2008). When the annual mean of an ensemble of four satellite-based precipitation products was compared to annual means of field observations at different weather stations the margin of either underestimation or overestimation was reduced (See Table A1 in supplementary data). To this extent, for the general water balance, this study used annual mean of four satellite precipitation products. The four precipitation products are the Climate Forecasting System Reanalysis (CFSR), Climate Hazards Group Infra-Red Precipitation with Station data (CHIRPS), ECMWF Reanalysis v5 (ERA5) and TerraClimate (see Table 1). These satellite precipitation products were selected purely based on availability and the fact that they are spatially distributed and cover the entire Luangwa Basin (Table 1). Field observations of precipitation for GART Chisamba (data for the period 2020 – 2022) and Lusaka International Airport, Kabwe, Mwinilunga and Serenje weather stations for the years 2014 - 2016 were obtained from the Southern African Science Service Centre for Change and Adaptive Land Management (SASSCAL) weathernet (Last accessed: 20 January, 2023: http://www.sasscalweathernet.org). The observations for Mpika for the year 2021 were obtained from the ZAMSECUR project dataset available at 4TU.ResearchData repository (https://doi.org/10.4121/19372352.v2) (Zimba *et al.*, 2022). Three weather stations, GART Chisamba, Lusaka International Airport and Mwinilunga, are outside of the Luangwa Basin and were used for comparison purposes only. However, GART and Lusaka International airport stations are very close to the Luangwa Basin. The other three stations Kabwe, Serenje and Mpika are within the Luangwa Basin (see Table A1 in the supplementary data for location coordinates of the weather stations). Nevertheless, the results of the comparison of satellite precipitation products with field observations were similar

(underestimation or overestimation) at all weather stations both in the Luangwa Basin and outside the basin (See Table A1 in the supplementary data).

Estimating runoff data

Reliable monthly basin-scale field observations of runoff were only available for the period 1961 -1992 and not for the study period 2009 – 2020. Monthly modelled TerraClimate runoff data (Abatzoglou *et al.*, 2018) was available for the period 1958 – 2020. Compared to field observations TerraClimate runoff data was significantly higher during the peak rainfall period of January-February. At annual scale TerraClimate overestimated runoff data but strongly correlated (r = 0.83) with field observations (Fig. 4a).

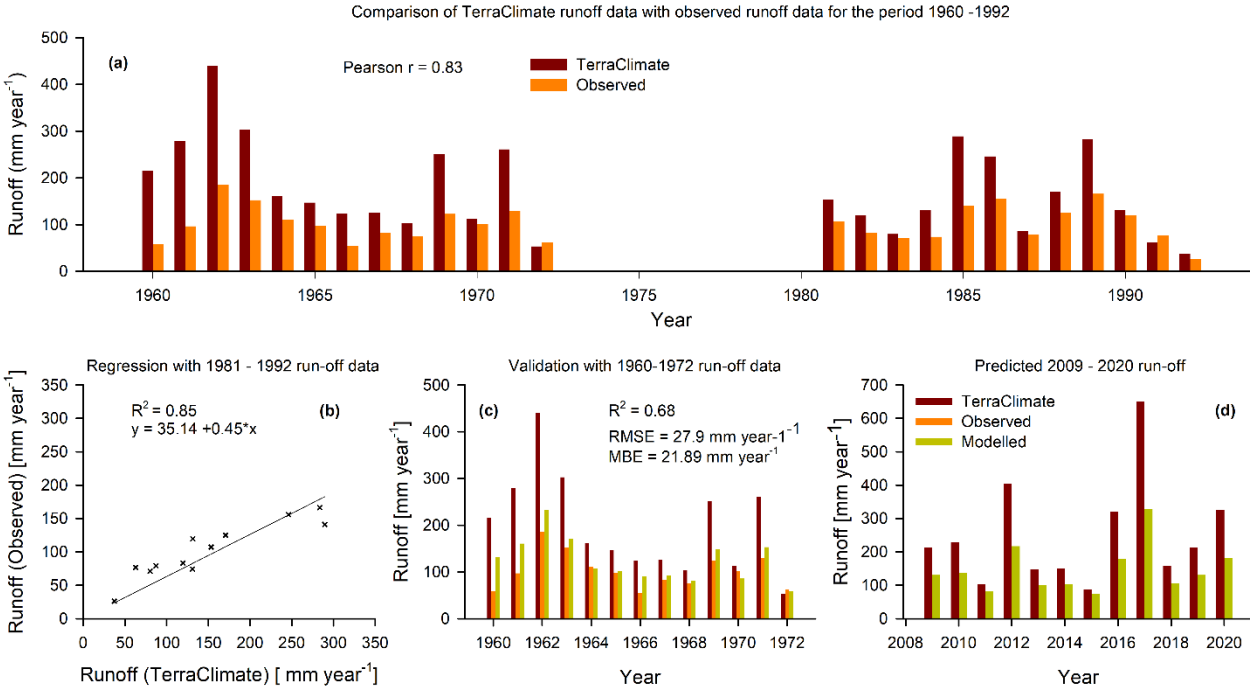

Figure 4: Procedure for extending near field observations runoff data for the period 2009-2020 using the TerraClimate runoff data as the predictor.

Based on the correlation of annual TerraClimate runoff data with field observations a linear regression equation was formulated to help generate extended near field observations time series for the period 2009-2020. TerraClimate runoff data was used as predictor variable. The TerraClimate runoff data was used because of availability free of cost and with relatively fine temporal and spatial resolution (monthly and 4 km respectively) (Table 1). Firstly, the field observations runoff data and TerraClimate runoff data for the period 1960 - 1992 were split into two segments, 1960 - 1972 and 1981 - 1992. The runoff data for the period 1981 -1992 was used as training data to generate a linear equation with the TerraClimate runoff data as the predictor variable (Fig. 4b). The generated linear equation was validated using the 1961-1972 TerraClimate runoff data as a predictor variable (Fig. 4c). The predicted 1961-1972 runoff data with the TerraClimate runoff data as a predictor variable was then compared to the field observations for the same period (Fig. 4 c). The performance statistics of the equation showed $R^2 = 0.68$, RMSE =

27.9 mm year^{-1} and mean bias error (MBE) = 21.9 mm year^{-1} (Fig. 4 c). The linear regression equation was then used to generate near field observations runoff data for the period 2009 – 2020 with TerraClimate runoff data for the same period as the predictor variable (Fig. 4 d). Generally, both for the observed and extended time series (with TerraClimate data as predictor) the annual runoff coefficient was 11%. The near field observations extended runoff data was then used in the water balance approach, as explained in Section 2.2.4 Eq. (1), to estimate actual evaporation at basin level.

2.2.5 Time series pre-processing and statistical analyses

Before performing statistical analyses, the original time series of evaporation, LAI, NDVI, Soil moisture and air temperature were adjusted for seasonality. The centred moving average (CMA) and adjusted seasonal factor (ASF) approach was used to deseasonalise the time series (Ghysels, Osborn, and Rodrigues, 2006; Nelson *et al.*, 1999; Briuinger, Krishnaiah, and Cleveland ,1983).

The coefficient of variation (CV) (%) in Eq. (2) (Helsel *et al.*, 2020) was used to understand the extent to which the satellite-based evaporation estimates varied between each other for each phenophase. Furthermore, the analysis of variance (ANOVA) (Helsel *et al.*, 2020) and all pairwise multiple comparison procedures with the Tukey Test (Helsel *et al.*, 2020) were performed. The pairwise comparison assisted in observing the satellite-based evaporation estimates that were significantly similar or different in magnitudes in each phenophase. The correlations (similarity in temporal trends) among satellite-based evaporation estimates were assessed at monthly and annual scales using a non-parametric technique: the Kendal correlation test (Helsel *et al.*, 2020).

$$\mathrm{CV} = \frac{\bar{x}}{\bar{s}} \tag{2}$$

where $\bar{x}$ is mean of the observations and $\bar{s}$ the standard deviation. The higher the CV value, the larger the standard deviation compared to the mean, which implies greater variation among the variables. To establish the extent to which the satellite-based evaporation estimates underestimated or overestimated evaporation, relative to E_{wb}, the mean bias error (Eq. 3) is used:

$$MBE = \frac{1}{n}\sum_{i=1}^{n}(E_{s_i} - E_{a_{(wb)_i}}) \tag{3}$$

where n is the number of annual data used, $E_{a_{(wb)}}$is the water balance-based actual evaporation time series and E_s is the satellite-based evaporation estimates time series. The smaller the mean bias error value (positive or negative), the less the deviation of the predicted values from the water balance obtained values (Helsel *et al.*, 2020).

3 Results and discussion

3.1 Basin scale miombo woodland climate and phenological temporal trend(s)

Figure 5 shows Luangwa Basin miombo woodland (area delineated miombo woodland only in Fig. 1b) aggregated 2009-2020 MODIS NDVI and CFSR data climate conditions: net radiation (R_N), air temperature (T_a), relative humidity (RH), soil moisture (SM) and precipitation (P). The peak atmospheric and phenological variables values were observed in the early and mid-rainy seasons during the green-up and maturity/peak phenophases. The lowest values in

atmospheric and phenological variables were observed in the cool dry season during the green-down and dormant phenophases. Net radiation, air temperature, relative humidity covaried (positively or negatively) with the NDVI (proxy for canopy phenology) depending on the phenophase (Fig. 5 and Fig. A2 in the supplementary data).

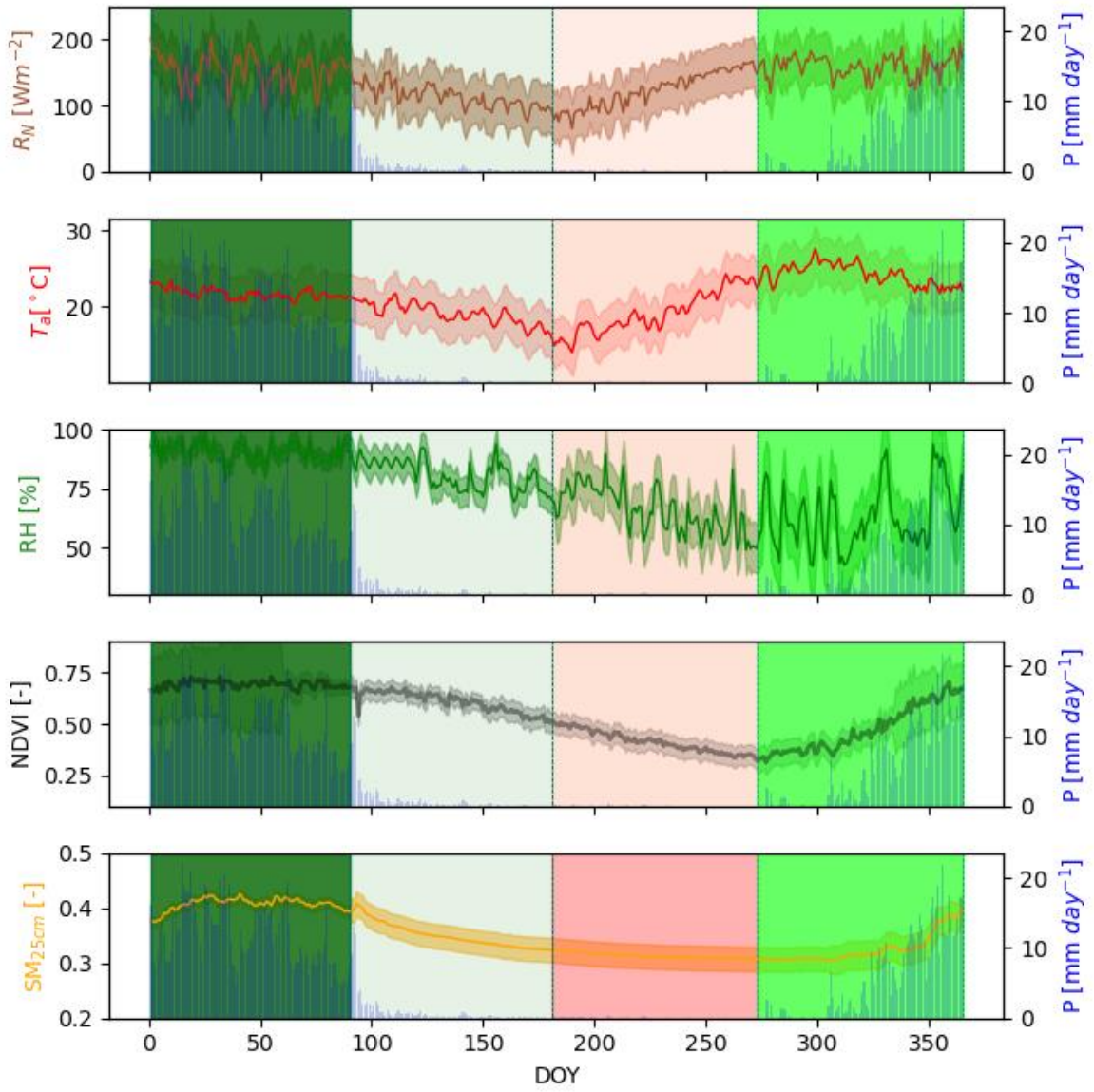

Figure 5: Luangwa Basin miombo woodland spatially and temporally aggregated 2009-2020 daily atmospheric conditions: net radiation (R_N), precipitation (P), relative humidity (RH) and air temperature (T_a); phenological conditions proxied by the NDVI; and soil moisture (SM). The shaded areas represent the phenophases as used in this study: January – March is the peak/maturity, April – June is the senescence/green-down, July – September is the dormant and October – December is the green-up/mid-green-up phenophase. Shaded area for variables is the standard deviation. DOY is the day of the year.

The strong correlation between climate and phenology (i.e., NDVI and air temperature/soil moisture) in the miombo woodland (Fig. A2 in the supplementary data) agreed with observations made by Chidumayo (2001) and in other ecosystems (Pereira *et al.*, 2022; Niu *et al.*, 2013; Cleland *et al.*, 2007).

3.2 Observed phenological conditions in the miombo woodland

It was observed that the canopy closure is varied, ranging between 2 percent to about 70 percent in the shrub, dry miombo woodland and wet miombo woodland (Fuller, 1999). Therefore, depending on location and dominant species, exposure of the understorey, field, and ground layers to incident solar radiation through the canopy is substantial (Fig. 6, Chidumayo, 2001; Fuller, 1999).

Figure 6: Dry season (a) and rainy season (b) tree layer, understorey, and field layer conditions at the wet miombo woodland site in Mpika, Zambia. Images taken on 29th September and 23rd December, 2021.

The field layer during the rainy season mainly comprises green grass (Fig. 6b and Chidumayo, 2001). Therefore, total LAI and NDVI in phenophases in the rainy season can be largely attributed to both the field layer i.e., grass, understorey, and the tree layer, i.e.: shrubs and tree canopy (i.e., Fig. 6b and Chidumayo, 2001). In the dry season, the grass in the field layer and some understorey non-deep rooting shrubs dry out (Fig. 6a and Chidumayo, 2001, Fuller, 1999). Therefore, the changes in total LAI and NDVI in the phenophases in the dry season can largely be attributed to the changes in the tree layer of the miombo species (i.e., Fig. 6a, Fig. 7 and Chidumayo, 2001). The LAI and NDVI were used as proxies to observe the changes in the canopy cover across different phenophases of the miombo woodland. At a 27.7km-by-27.7km grid scale (Fig. 8a) the spatial distribution and mean values of the LAI and NDVI for the wet miombo woodland differed with that for the dry miombo woodland (Fig. 8a). This difference is due to the differences in species composition and distribution at each site. Furthermore, there are differences in soil type, soil moisture, temperature, nutrients, rainfall, and canopy closure at the two sites (i.e., Chidumayo, 2001; Fuller, 1999). However, trends in the NDVI and LAI across different phenophases of the miombo woodland at the two sites were similar ($r = 0.73$ for LAI and NDVI respectively) (Fig. 8b). Highest LAI and NDVI, both in the dry miombo woodland and wet

miombo woodland, were observed in the maturity/peak phenophases during the mid-rainy season (January – March) (Figs. 5, 7 & 8c and Fig. A3 in the supplementary data).

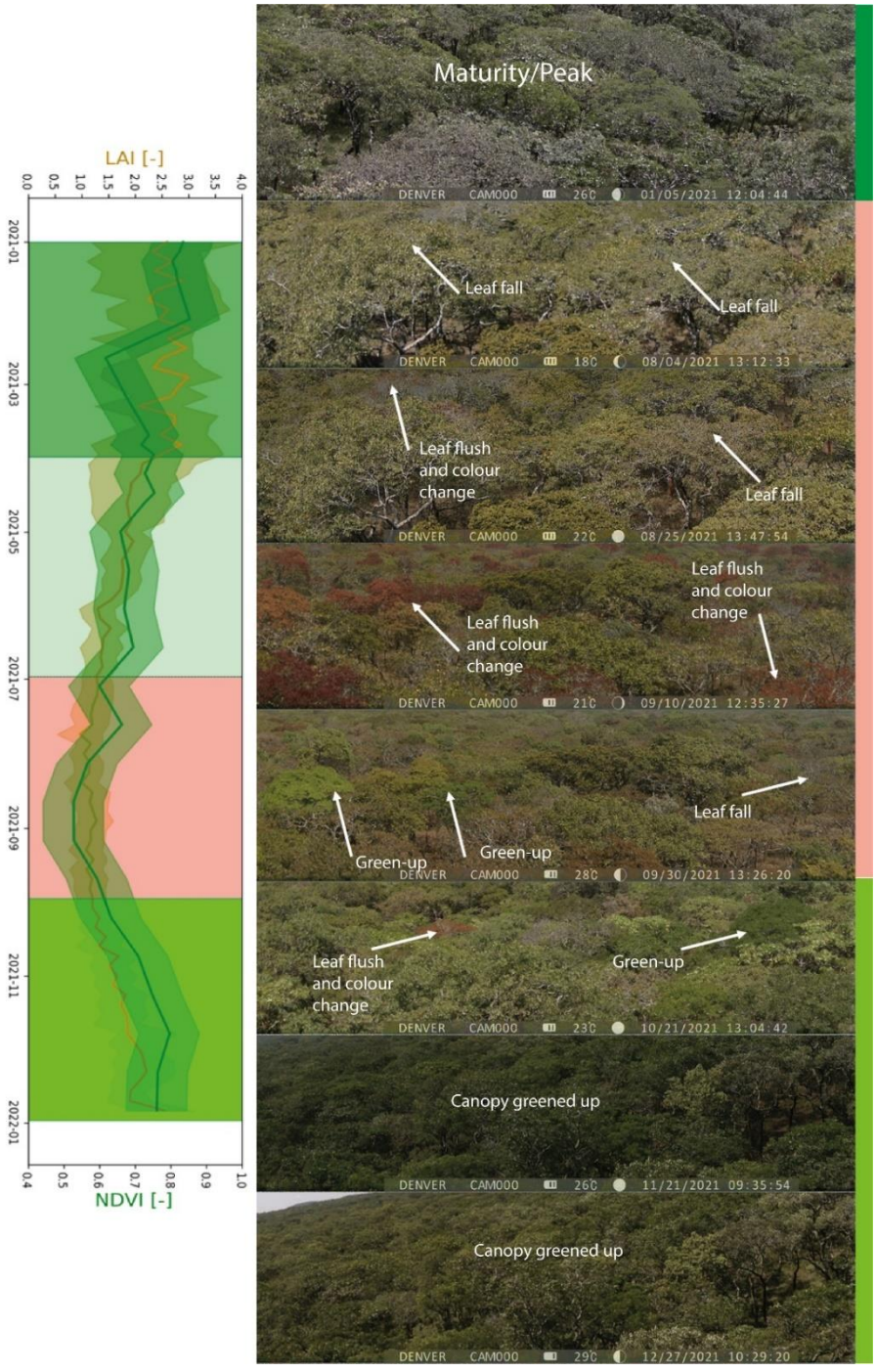

Figure 7: Temporal trend of MODIS *LAI*, *NDVI*, and the wet miombo woodland canopy display trend for the year 2021 at Mpika study site. Shaded area are phenophases: January – March is the Maturity/Peak; April-June is the Senescence/Green-down; July-September is the Dormant while October – December is the green-up. Shaded area for variables is the minimum and maximum.

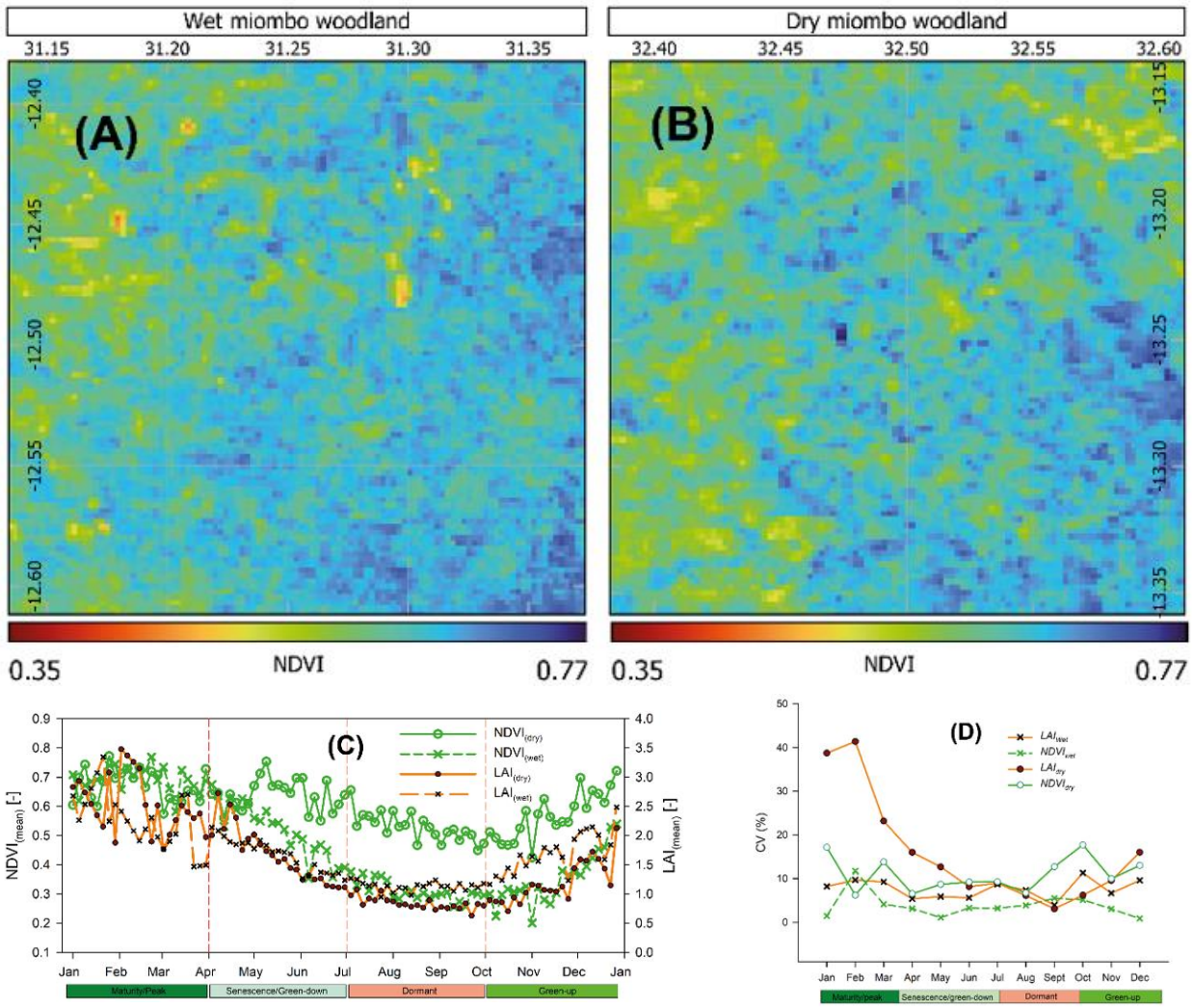

Table 2. Dormant phenophase CV correlation

Variables	LAI (wet)	NDVI (wet)	LAI (dry)	NDVI (dry)
LAI (wet)	**1**			
NDVI (wet)	**-1.00**	**1**		
LAI (dry)	0.98	-0.98	**1**	
NDVI (dry)	-0.75	0.75	-0.59	**1**

Figure 8: Spatial distribution of NDVI at the (A) wet miombo woodland and (B) dry miombo woodland site for the period January-December, 2021. (C) Temporal distribution of the LAI and NDVI for the wet miombo woodland and dry miombo woodland. (D) Coefficients of variation in the LAI and NDVI values at the wet miombo woodland and dry miombo woodland in the Luangwa Basin in Zambia for the year 2021.

This period for peak LAI and NDVI (Figs. 7 & 8) agrees with Chidumayo (2001) who observed that peak green biomass in the miombo woodland occur anytime between January and May. The lowest LAI and NDVI were observed in the dormant phenophase in August/September during the warm pre-rainy season (Figs. 5, 7 & 8).

The leaf-fall, leaf-flush and changes in colour of the leaves intensifies in the August-September period (Fig. 7, Chidumayo, 2001; Chidumayo and Frost, 1996; Fuller, 1999). The intensified leaf-fall, leaf-flush and leaf colour changes may also explain the increased variations in the NDVI values in August-September (Fig. 8d). Table 2 shows the correlation coefficients of the coefficients of variations in NDVI and LAI values for the dry miombo woodland and wet miombo woodland.

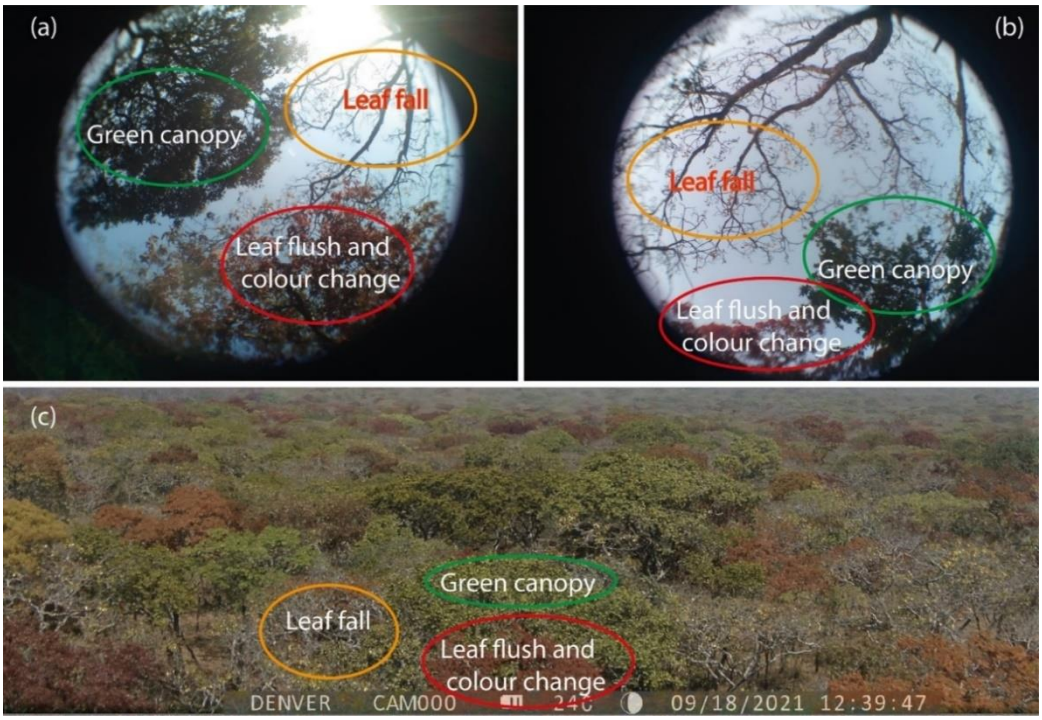

Figure 9: Heterogeneity in leaf-fall and leaf-flush activities among miombo woodland species: observed from under the canopy (a, b) and as observed above the canopy (c). Images taken at the wet miombo woodland site in Mpika, Zambia. Images taken on 18 September, 2021.

The coefficients of variation in LAI and NDVI values for the dry and wet miombo woodland were only similar for the dormant phenophase (r = 0.98 and 0.75 for the LAI and NDVI respectively (Fig. 8 and Table 2). This similarity in the dormant phenophases may be due to the plants undergoing similar phenological processes; leaf-fall and leaf-flush. In the dormant phenophase the grass component would have dried out, leaving the tree component (i.e., the canopy) to determine the leaf area (Chidumayo, 2001).

The coefficients of variation of LAI values in July and August over the wet miombo woodland can be attributed to increased leaf-fall activity (Fig. 8). Fuller (1999) observed that in the wet miombo woodland the co-occurrence of leaf-fall and leaf-flush, in August and September, resulted in net zero change in the canopy closure. The net zero change increase in canopy closure may explain the observed low coefficient of variation of the LAI values in September (Fig. 8). The

high coefficient of variations of LAI and NDVI values, for both dry miombo woodland and wet miombo woodland, during the mid-rainy season in the maturity/peak phenophase can be attributed to two factors: firstly, the heterogenous growth of the green biomass of the woodland which occurs anytime between January and May (Chidumayo, 2001, Fuller, 1999) and the effect of cloud cover on the quality of the satellite-based LAI and NDVI products (Vermote and Wolfe, 2015; Zang *et al.*, 2003). Furthermore, the differences in the canopy closure between the dry miombo woodland and wet miombo woodland (Fuller, 1999) may be the reason for differences between the coefficients of variations in LAI and NDVI values in the maturity/peak and senescence\green phenophases. For instance, the dry miombo woodland, which has a lower canopy closure compared to the wet miombo (Fuller, 1999), is likely to have a higher grass component. Additionally, the differences in miombo species composition, distribution of rainfall, soil type and soil moisture, among other variables, may result in varied phenological differences between the dry miombo woodland and wet miombo woodland (Chidumayo, 2001; Fuller, 1999).

3.3 Phenophase-based difference in satellite-based evaporation estimates

3.3.1 Correlation of satellite-based evaporation estimates

Figure A3 in the supplementary data shows the temporal distribution of evaporation in relation to the proxy of woodland canopy cover (i.e., NDVI) and rainfall across phenophases in a hydrological year of the Luangwa Basin. The highest satellite-based evaporation estimates were observed during the rainy season (with highest NDVI values) while the lowest were in the dry season (with lowest NDVI values) (Fig. A3 in the supplementary data).

Time series of satellite-based evaporation products and proxies (LAI and NDVI) for woodland canopy cover for the Luangwa Basin miombo woodland were adjusted for seasonality (Fig. 10). The original time series and the seasonally adjusted time series for the dry miombo woodland and wet miombo woodland are shown in Fig. A4 in the supplementary data.

For analysis the data were segmented based on climate phenophases and satellite-based phenophases (Fig. 2 and as described in Section 2.2.1).

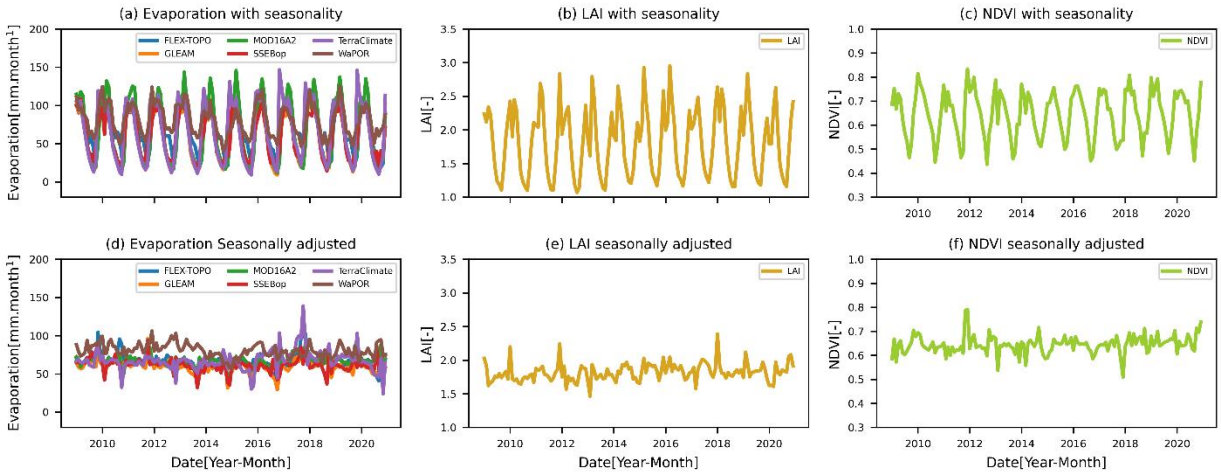

Figure 10. Original non-stationary time series and seasonally adjusted (deseasonalised) time series for the miombo woodland in the Luangwa Basin: a, d is the evaporation, b, e is the LAI and c, d is the NDVI.

With reference to both non-stationary and stationary time series, in different phenophases, each satellite-based evaporation estimate appeared to correlate differently with other evaporation estimates (Figs. 11, 12 and Figs. A5 – A8 in the supplementary data). For instance, in the warm dry season/dormant phenophase, FLEX-Topo and WaPOR had, generally, lower correlations with the rest of the satellite-based evaporation estimates (Figs. 11, 12 and Figs A5 – A8 in the supplementary data).

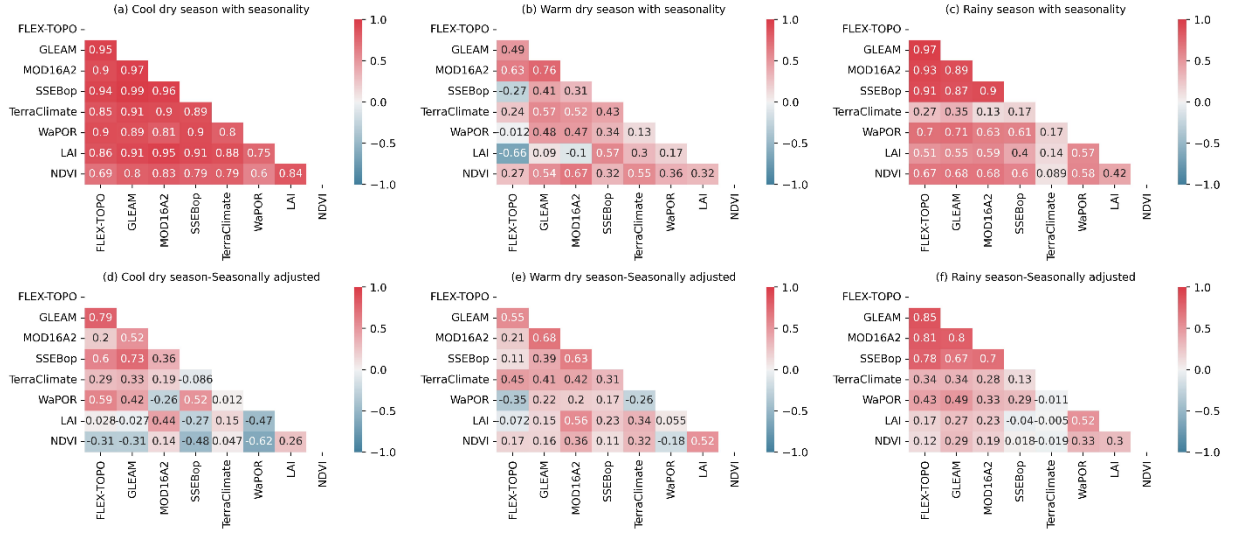

Figure 11. Climate-based phenophases correlation of satellite-based evaporation estimates and proxies (LAI and NDVI) for woodland canopy cover for the miombo woodland in the Luangwa Basin: (a)-(c) original non-stationary time series with seasonality, (d) – (f) seasonally adjusted time series.

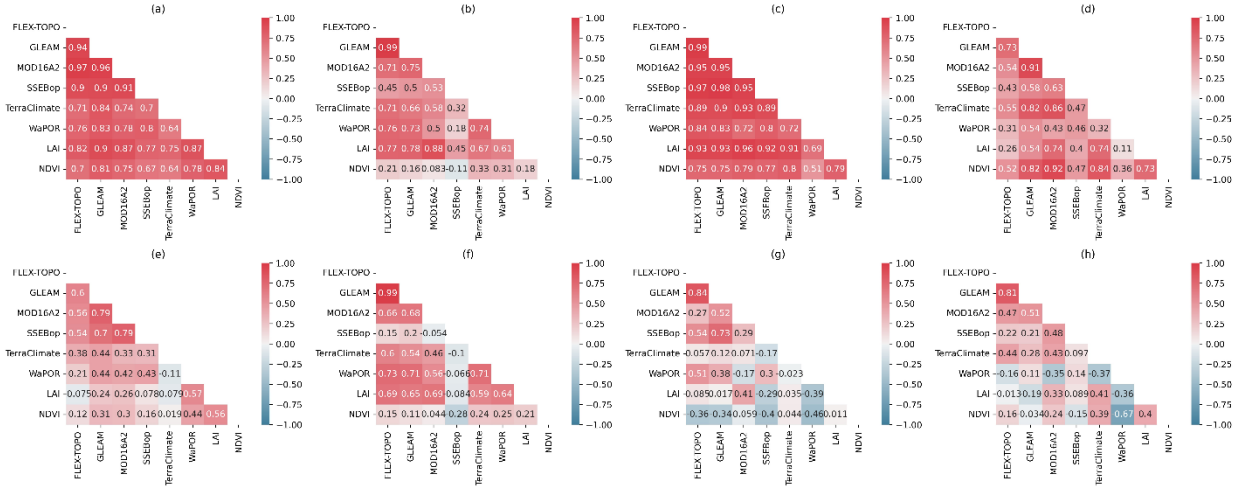

Figure 12. Satellite-based phenophases correlation of satellite-based evaporation estimates and proxies (LAI and NDVI) for woodland canopy cover for the miombo woodland in the Luangwa Basin: (a-d) original time series with seasonality, (e) – (h) seasonally adjusted time series. (a, e) green-up/mid-green-up, (b, f) maturity/peak, (c, g) senescence/green-down/mid-green-down, (d, h) dormant.

However, with both non-stationery time series (with seasonality) and stationary (seasonally adjusted) time series, significant stronger ($r > 0.5$, p-value < 0.05) correlations among the satellite-based evaporation estimates were observed during the rainy season and immediately after the rains in the cool dry season. Significant weaker ($r < 0.5$, P-value < 0.05) correlations were observed during the warm dry season/dormant phenophases (Figs.11,12 and Figs. A5 - A8 in the supplementary data).

Stronger correlations among satellite-based evaporation estimates appears to be during periods with high woodland leaf area, high soil moisture content and high vegetation water during the rainy season and cool-dry season (Figs. 5, 7, 11 & 12). The same pattern of correlation of satellite-based evaporation estimates observed for the miombo woodland at the Luangwa Basin scale was observed for both the dry miombo woodland and wet miombo woodland (Figs. A5 – A8 in the supplementary data).

To the contrary, the lowest correlation coefficients among satellite-based evaporation estimates appear to be during water stressed period(s) in the warm dry season (Figs. 5, 7, 11 & 12). Generally, compared to time series with seasonality, the seasonally adjusted time series gave lower coefficients of correlation among the satellite-based evaporation estimate across seasons and phenophases (Figs. 11, 12).

3.3.2 Temporal variations in satellite-based evaporation estimates across phenophases

Across phenophases (climate and satellite-based) comparison of the means of the seasonally adjusted time series of satellite-based evaporation estimates did not show large differences (< 0.5% difference) in the coefficients of variation of estimates (Figs. 13, 14 & Fig. A9 in the supplementary data). It appears that when seasonality is removed the means of satellite-based evaporation estimates show minimal different across phenophases with relatively higher coefficients of variation in the warm dry season phenophase/dormant phenophase and cool dry season/senescence phenophase (Figs. 13, 14 & Fig. A9 in the supplementary data).

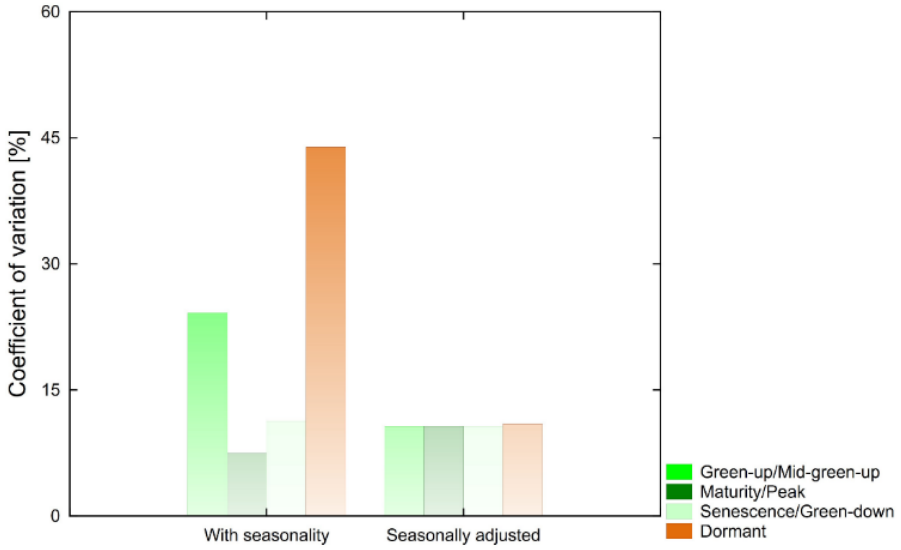

Figure 13. Satellite data-based phenophases coefficients of variation of estimates of satellite-based evaporation estimates for non-stationary time series and seasonally adjusted time series for the miombo woodland in the Luangwa Basin.

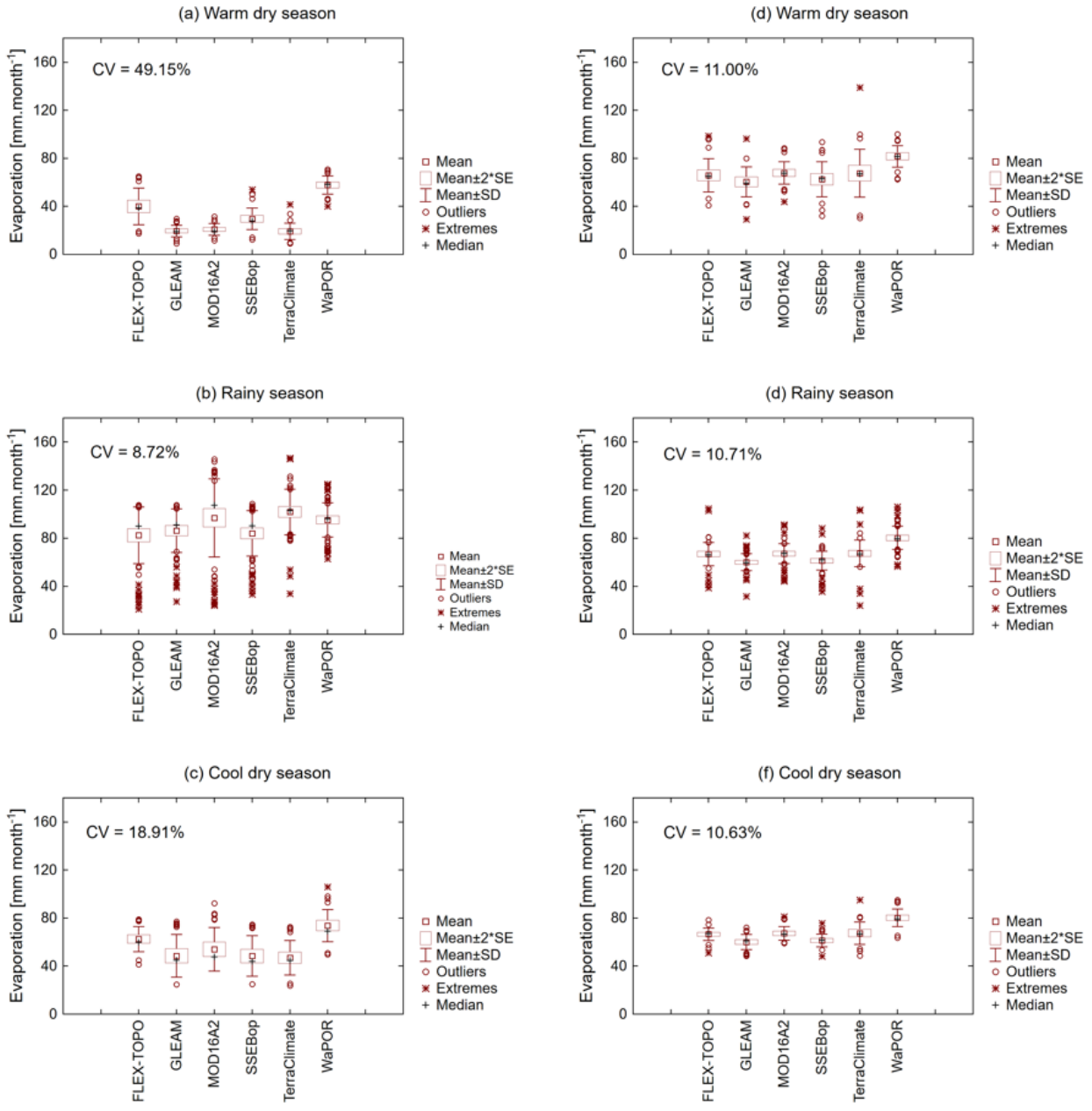

Figure 14: Box plots comparing satellite-based evaporation estimates, (a-c) with seasonality and (c-f) with seasonally adjusted time series, across climate-based phenophases of the miombo woodland for the period 2009 - 2020 in the Luangwa Basin. The coefficient of variation (CV) is for the comparison between the six satellite-based evaporation estimates.

The dry season coefficients of variations in evaporation estimates could be indicative of the possible influence of the adapted water limited conditions buffering mechanisms by the miombo species. Across phenophases the WaPOR showed the highest estimates of evaporation while GLEAM consistently showed the lowest mean estimates (Fig. 14 d- f). For instance, the canopy cover at the wet miombo woodland (Figs. 7 & 9) remained high (i.e., as evidenced in the satellite-based NDVI mean values of around 0.55 in Fig. 7). With the highlighted adapted attributes

of the miombo species for the dry season it is probable that inadequate representation in satellite-based evaporation estimates could result in varied estimates of transpiration.

Furthermore, time series with seasonality showed significant differences in the coefficients of variation between phenophases with the largest observed in the warm dry season (i.e., CV = 49.15 %; 43.90 % for the warm dry season and dormant phenophases respectively) (Fig. 13, 14 & Fig. A9 in the supplementary data). For the warm dry season/dormant phenophase, the lower coefficients of correlation and higher coefficient of variation (i.e., 49.15 %) could indicate that while the temporal trends among some of the satellite-based evaporation estimates are similar ($r > 0.5$) (Figs. 11 & 12), the amounts of evaporation estimates are significantly different (CV > 40%) (Figs. 13, 14 & Fig. A9 in the supplementary data). The occurrence in the warm dry season of higher coefficients of variation, with both non-stationary times series and seasonally adjusted time series, consolidates the possible role of the adapted phenological and physiological attributes of miombo species on evaporation.

In contrast, for the rainy season/maturity/peak phenophase, except for the SSEBop and TerraClimate, the temporal trends among satellite-based evaporation estimates were largely similar ($r > 0.5$) and the magnitudes of evaporation estimates not very different (CV = 8.72 %; 7.46% for the rainy season and maturity/peak phenophases respectively) (Figs. 11, 12, 13, 14 & Fig. A9 in the supplementary data).

Compared to the warm dry season the cool dry season/senescence/green-down phenophases showed higher correlations ($r > 5$) and lower differences in the magnitudes of estimates of satellite-based evaporation estimates (CV = 18.9 %, 11.29% for the cool dry season phenophase and senescence/green-down phenophase respectively) (Figs. 11, 12, 13, 14 & Fig. A9 in the supplementary data). The results for the senescence/Green-down phenophase appear to agree with the findings by Zimba *et al.* (2023) in which they showed, at point scale, that for these phenophases the temporal trends and magnitudes of satellite-based evaporation estimates were similar to each other and also to the field observations of actual evaporation in the wet miombo woodland.

In the warm dry season/dormant phenophase the WaPOR, followed by FLEX-Topo, showed higher estimates of evaporation compared to other satellite-based evaporation estimates (Figs. 14 & A3, A9 in the supplementary data). Zimba *et al.* (2023) showed, at point scale in the wet miombo woodland, that satellite-based evaporation estimates underestimated actual evaporation in the warm dry season. They also showed that while the NDVI was generally in a downward trajectory from May to September, the observed actual evaporation had a rising trajectory which was in agreement with the rising air temperature and net radiation. Compared to other satellite-based estimates the WaPOR followed the same temporal trend as the field observations of actual evaporation of the wet miombo woodland in the dry season (Zimba *et al.*, 2023). In this study, WaPOR showed negative correlation with the LAI/NDVI in the warm dry season/dormant phenophases (Figs. 11d, e &12g, h). Therefore, with reference to findings by Zimba *et al.* (2023) and Figs. 11 & 12, the WaPOR appear to have the correct temporal trend of actual evaporation of the miombo woodland in the cool dry season/ senescence/green-down and the warm dry season/dormant phenophases.

The green-up phenophase is at the start of the rainy season with increasing LAI and high canopy cover (i.e., mean NDVI between 0.5 and 0.7) and highest net radiation (i.e., 150 Wm^{-2}) (Figs. 5, 7 & 9). The dormant phenophase is during the driest part of the year with the lowest moisture in the topsoil, least woodland canopy cover (i.e., NDVI $\approx$ 0.5) but, compared to the senescence/green-down phenophase, with increasing net radiation and air temperature (Figs. 5, 7

& 9).

What is important to note is that, unlike during the maturity/peak and senescence/green down phenophases, the total LAI and total NDVI during the dormant and early green-up phenophases can largely be attributed to the tree layer (i.e., miombo woodland canopy) (Fig. 6; Chidumayo, 2001; Chidumayo and Frost, 1996). The implication of the total LAI and NDVI in the dry season is that the dormant and early green-up phenophases are likely to be more representative of the evaporation of the miombo species than the other phenophases in the rainy season and early dry season (cool dry season) when the green grass component is substantially high. Compared to the maturity/peak and the senescence/green-down phenophases, the dormant and green-up phenophases showed higher coefficients of variations in evaporation estimates among satellite-based evaporation estimates (Figs. 13 & 14).

The comparatively higher coefficients of variation (Figs. 13 & 14) in the estimates of satellite-based evaporation estimates during the warm dry season suggests that there are aspects of the evaporative processes (i.e., adapted phenological and physiological attributes of the miombo species that are possibly not taken into account in satellite-based evaporation estimates. The possible explanations for the observed temporal trends (i.e., correlations) and coefficients of variations in the satellite-based evaporation estimates are given in section 3.5.

3.3.3 Spatial distribution of satellite-based evaporation estimates across phenophases

Figure 15 shows spatial-temporal distribution of satellite-based evaporation estimates across different phenophases for the hydrological year 2019/2020. The comparison was based on the entire Luangwa Basin, including non-miombo woodland regions. Generally, the spatial distribution and detail of evaporation estimates are different, but, like the temporal trends, they are most pronounced in the dormant and green-up phenophases (Figs. 13, 14 & 15). During periods of high soil moisture and high leaf area (i.e., Figs. 5 & 7), in the maturity/peak and senescence/green-down phenophases, the products are more in agreement. It can further be seen that during the dormant phenophase, all six evaporation estimates showed higher actual evaporation in wooded areas (Fig. 15) (refer to Fig. 1 b, c for the cover of the miombo woodland in the Luangwa Basin). Potential contributing factors to the observed differences in spatial-temporal distribution of satellite-based evaporation estimates are highlighted in section 3.5.

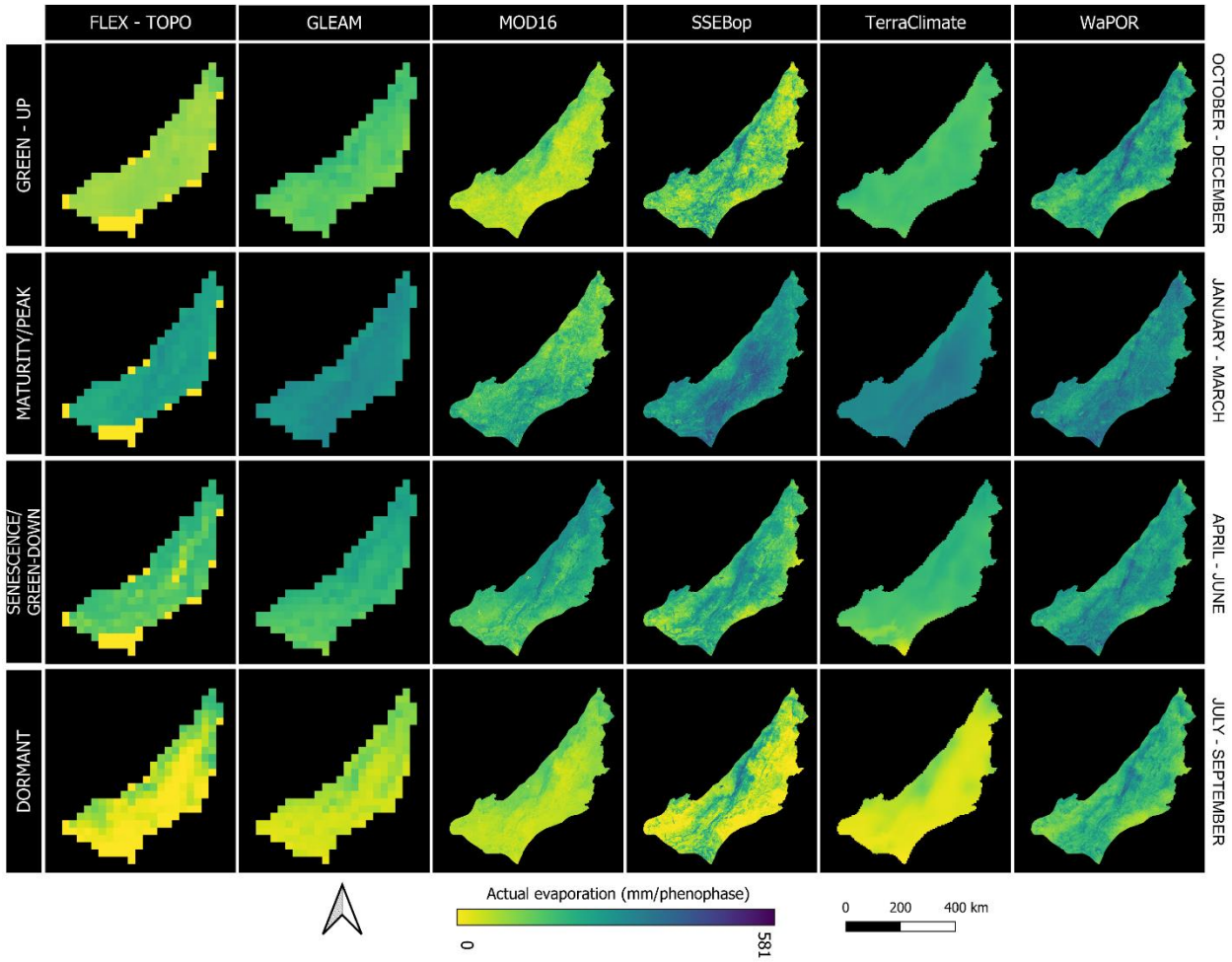

Figure 15: Spatial-temporal distribution of satellite-based evaporation estimates across different vegetation phenophases of the Luangwa Basin for the hydrological year September 2019 - August 2020.

3.3.4 Pairwise multiple comparison of satellite-based evaporation estimates at Luangwa Basin miombo woodland scale

It appeared there are no statistically significant differences in the estimates of evaporation for the dry miombo woodland and wet miombo woodland by each satellite-based evaporation estimate (Fig. A10 and Tables A2 in the supplementary data). Therefore, the all pairwise comparison was performed only for the entire miombo woodland of the Luangwa Basin. Tables A4 and A5 in the supplementary data shows the results of the all pairwise multiple comparison of satellite-based evaporation estimates with seasonality (Table A4) and the seasonally adjusted time series (Table A5 in the supplementary data). For both time series, it appeared the WaPOR estimates were the most different across phenophases (Fig. 16). The other satellite-based evaporation estimates with mean estimates significantly different from other estimates, after the WaPOR, are the FLEX-Topo, followed by the MOD16 and TerraClimate (Fig. 16, Tables A4 & A5 in the supplementary data).

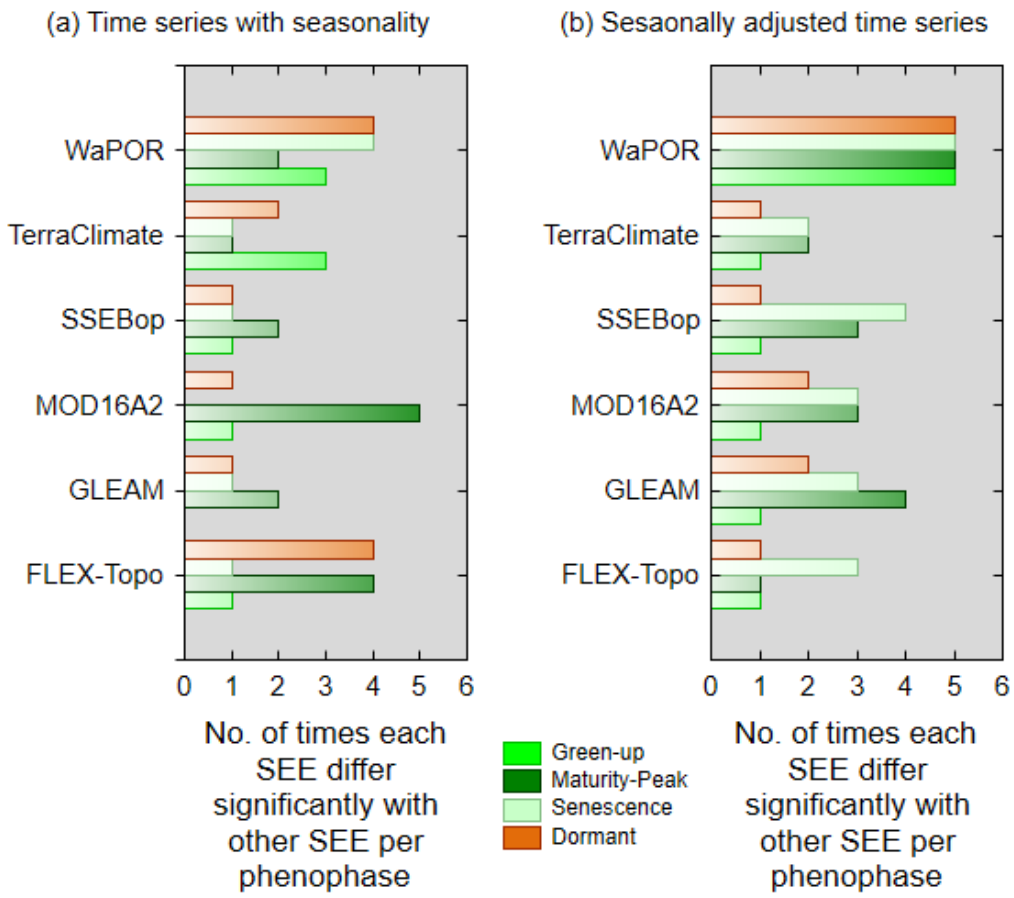

Figure 16: Number of times each satellite-based evaporation estimate (SEE) was significantly different to one or more other SSE in each phenophase at Luangwa Basin miombo woodland scale.

3.3.5 Variations within each climate, LAI, NDVI and satellite-based evaporation estimate

With the exception of WaPOR, monthly temporal variations of satellite-based evaporation estimates were highest during the green-up phenophase, followed by the dormant and senescence/green-down phenophases (Fig. 17). The maturity/Peak showed the lowest coefficients of variations of satellite-based evaporation estimates (Fig. 17 and Table A3 in the supplementary data). The green-up and senescence/green-down phenophases are at the boundaries of the dry season into the mid-rainy season (in case of green-up phenophase) and the rainy season into the dry season (in the case of the senescence/green-down phenophase). The coefficients of variation of the NDVI (i.e., canopy cover), rainfall (i.e., water availability) and temperature (i.e., energy availability) in the green-up and senescence/green-down phenophases (Fig. 17) likely explains the temporal variations in each satellite-based evaporation estimates. The phenophases in which the LAI, NDVI, rainfall and soil moisture appear to show larger coefficients of variations are also the phenophases in which individual satellite-based estimates show higher coefficients of variation (Fig. 17). The temporal variation of satellite-based evaporation estimates in the dormant phenophase could be as a result of the changes in the canopy cover due to the leaf-fall, leaf-flush and leaf colour changes (i.e., NDVI as shown in Figs. 7, 9 & 17). Figure 17 generally shows that the variations in LAI, NDVI, rainfall, soil moisture and air temperature are mirrored in the variations of the satellite-based evaporation estimates.

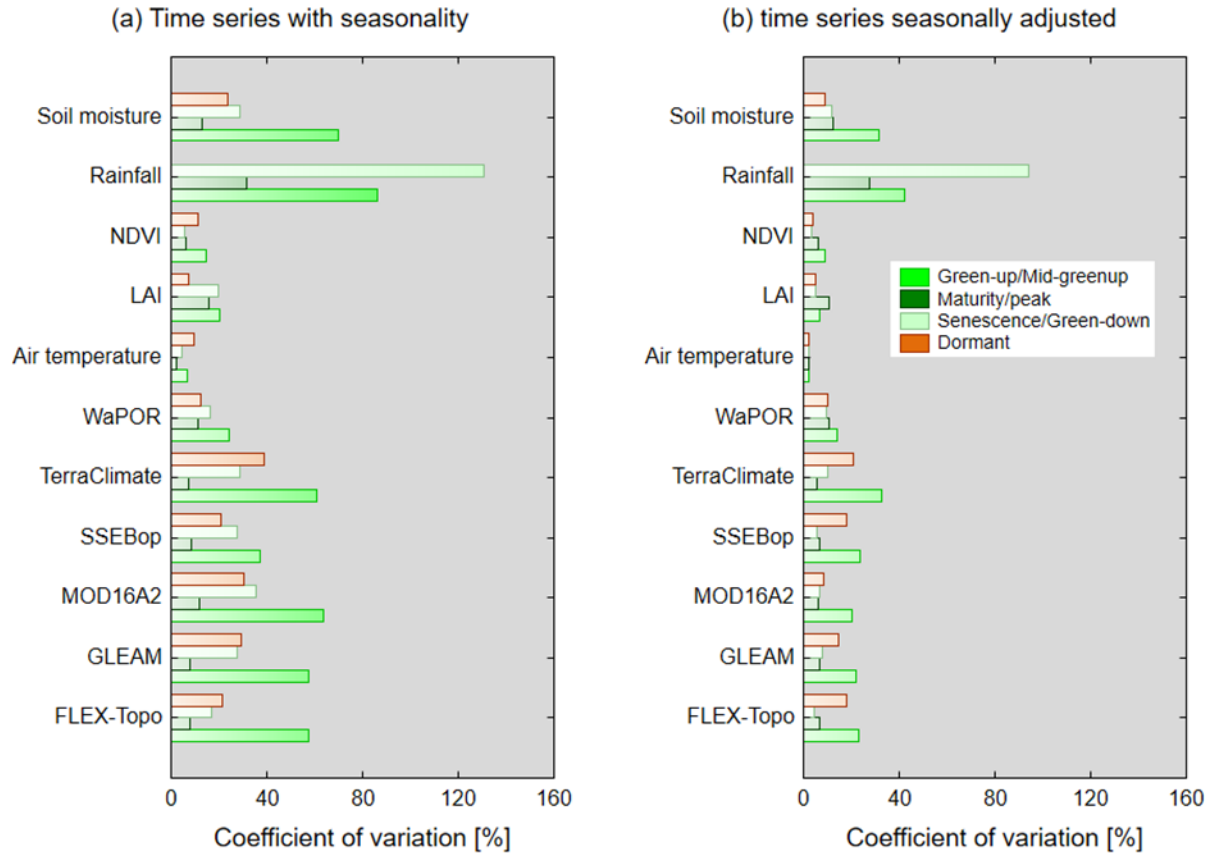

Figure 17: Coefficients of variations for (a) time series with seasonality and (b) seasonally adjusted time series across phenophases for the miombo woodland, Luangwa Basin.

3.4 Comparison of satellite-based evaporation estimates to the water balance-based actual evaporation

Figure 18 shows the temporal comparison of satellite-based evaporation estimates with the water balance-based actual evaporation of the Luangwa Basin for the hydrological years for the period September 2009 to August 2020. This comparison included non-miombo woodland areas. All satellite-based evaporation estimates showed insignificant correlation (*p-value* > 0.05) with the water balance-based actual evaporation (E_{wb}) (Fig. A11 in the supplementary data). Compared to the E_{wb} estimates, all six satellite-based evaporation estimates underestimated actual evaporation (Fig. 18a, b). The poor correspondence can be due to several factors.

Firstly, the disregard of over-year storage may explain the very low actual evaporation estimate in the dry year 2015. In that year the over-year storage should likely not be disregarded, and it is also possible that farmers in the cropland areas withdrew water from small dams. Taking these factors into account would have led to a higher actual evaporation estimate in 2015.

Secondly, the overall higher water balance-based actual evaporation may be due to the disregard of potential inter-basin groundwater exchange, or leakage of groundwater to the Zambezi. Hulsman et al. (2021) estimated that this leakage on average could amount to 143 mm/y.

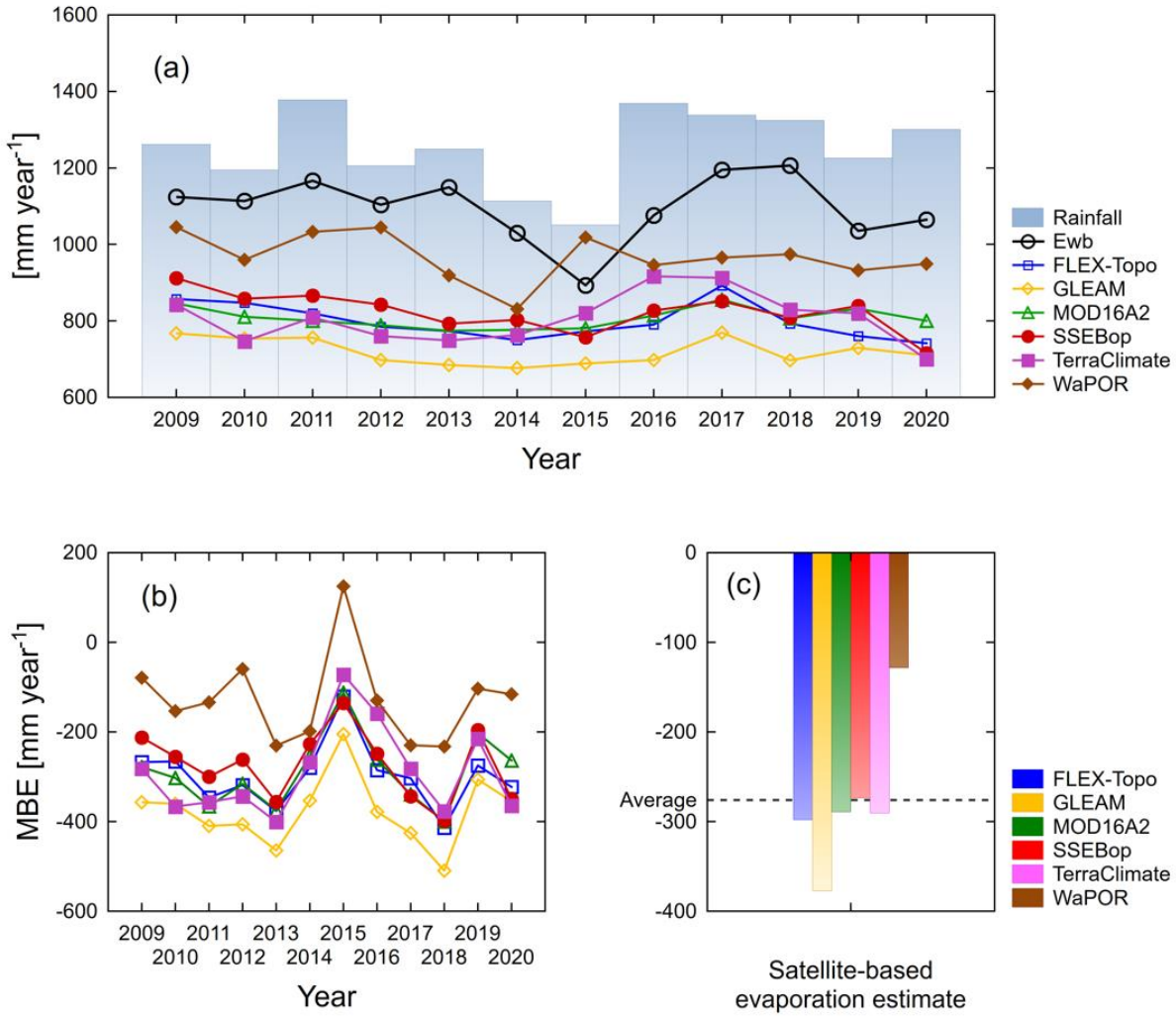

Figure 18: (a) Comparison of satellite-based evaporation estimates to the water balance-based estimate of actual evaporation for the Luangwa Basin, and (b) comparison of the MBE of satellite-based evaporation estimates for each year, and (c) comparison of the multi-year average MBE of individual satellite-based evaporation estimates.

This amount would be enough to bridge the bias between WaPOR and the water balance-based actual evaporation in Fig. 18c. Furthermore, there are uncertainties in the river discharge and the spatially averaged precipitation, which may have been over-estimated. The extended runoff time series with TerraClimate (Fig. 4 c, d) may have been overestimated resulting in underestimating the water balance-based actual evaporation at basin scale. The assumption of overestimation of the extended runoff data is based on the validation results of the linear equation used to extend the runoff time series, which showed RMSE = 27 mm year^{-1} and MBE = 21 mm year^{-1}.

In any given year, WaPOR appeared to have the least underestimation with an average MBE of 120 mm year^{-1}, while GLEAM had the largest underestimation with an average MBE of 370 mm year^{-1} (Fig. 18c).

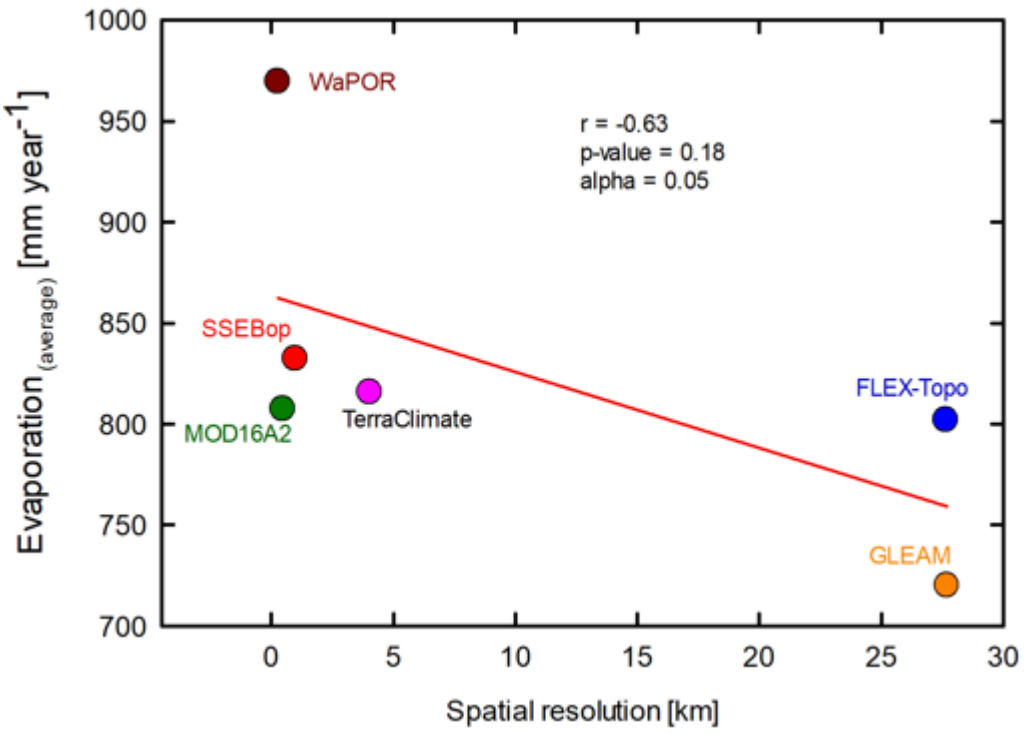

Figure 19. Luangwa Basin scale relationship between 2009-2020 annual averages of evaporation estimates and spatial resolution of satellite-based evaporation estimates.

At basin scale, it appeared there was no statistically significant correlation (r = -0.63; *p-value* = 0.18; alpha = 0.05) between spatial resolution and evaporation estimates of each product (Fig. 19). For instance, TerraClimate, with a coarser spatial resolution, showed similar bias estimates as SSEBop and MOD16. MOD16 had an even higher spatial resolution than SSEBop, but underestimated more. FLEX-Topo had a coarser spatial resolution than MOD16 and SSEBop but exhibited higher estimates in the warm dry season/dormant phenophases (Fig. 14 and Fig. A3 in the supplementary data). The lack of a clear relationship between spatial resolution and actual evaporation estimates (Fig. 19), may imply that other factors such as the heterogeneity in the land cover (i.e., miombo woodland, mopane woodland, cropland, settlements etc), access to soil moisture and groundwater, differences in model structure (such as the inclusion of leakage), processes and model inputs, as highlighted in Zimba *et al*. (2023) and section 3.5 in this study, may be the largest contributing factors of the observed differences in the actual evaporation estimates at basin scale.

However, the underestimation of actual evaporation at basin scale by satellite-based evaporation estimates cannot be entirely attributed to the inaccuracies in the simulation of miombo woodland evaporation. The evaporation of other vegetation types, i.e., mopane woodland, has not been investigated. The basin scale water balance-based comparison suggests that satellite-based evaporation estimates possibly underestimate actual evaporation also in non-miombo woodland landscapes. This requires more investigation of different landscapes and land covers such as grassland, shrubland, wetland and mopane woodland. For a more comprehensive understanding of the evaporation of the Luangwa Basin there is need for the assessment of the phenology-water

interactions of each vegetation type and the accompanying potential influence on the evaporation dynamics of the basin. Nevertheless, the results of this study agreed with Weerasinghe *et al.* (2020) who showed that most satellite-based evaporation estimates generally underestimate evaporation across African basins (i.e., Zambezi Basin). The lower underestimation by WaPOR agreed with the point scale field observations for the wet miombo woodland (Zimba *et al.,* 2023) and suggests that WaPOR is closest to actual evaporation of the miombo woodland in the Luangwa Basin.

3.5 Potential causes of differences in trends, magnitudes and spatial distribution of satellite-based evaporation estimates

Most pronounced differences in trends and magnitudes of satellite-based evaporation estimates of the miombo woodland have been observed in the dormant phenophase of the dry season (Figs. 11-16 & A3 in the supplementary data). Evaporation during that period is dominated by transpiration (i.e., Tian *et al.,* 2018). The dominant phenological characteristic of the miombo species in the dry season is the co-occurrence of leaf-fall, leaf-flush and greening up before commencement of seasonal rainfall (Figs. 7&9; Chidumayo and Frost, 1996; Frost, 1996) which affects transpiration (e.g., Marchesini *et al.,* 2015; Snyder and Spano, 2013). Tian *et al.* (2018) showed that the terrestrial groundwater storage anomaly (TWS) continued to decrease throughout the dry season and was indicative that miombo trees used deep ground water during that period. The suggestion that miombo trees access ground water is supported by Savory (1963) who showed that miombo species are deep rooting beyond 5 m with capacity to access ground water. Therefore, it is likely that satellite-based evaporation estimates using models whose structure, processes and inputs take into account the highlighted phenology-water interactions during the dry season and early rainy season, especially the access to deep soil moisture, would produce more accurate trends and magnitudes of evaporation in the miombo woodland.

3.5.1 Use of proxies for soil moisture

Some studies have shown that direct integration of soil moisture rather than the use of proxies improves the accuracy of actual evaporation estimates (Brust *et al.,* 2021; Novick *et al.,* 2016). The challenge with the use of proxies for soil moisture, for example in surface energy balance models, is that these are unable to fully account for changes in other factors that may influence sensible heat fluxes (Gokmen *et al.,* 2012). To improve the accuracy of estimation of water and energy fluxes in regions with recurrent plant water stress, such as in miombo woodland, Gokmen *et al.* (2012) suggested that the soil moisture be integrated in surface energy balance models. For instance, for MOD16 the use of the relative humidity and vapour pressure difference as proxies for soil moisture maybe a source of uncertainty in estimating transpiration (Novick *et al.,* 2016). Direct integration of soil moisture into the MOD16 algorithm appeared to improve the accuracy of actual evaporation estimates (Brust et *al.,* 2021). The energy balance-based SSEBop does not explicitly consider soil moisture dependency and assumes that the variations in satellite-based land surface temperature and vegetation indices, such as the NDVI, accounts for soil moisture (Senay *et al.,* 2013). TerraClimate uses the plant-extractable water capacity of soil for soil moisture input. However, the difficulty in determining the plant-extractable water capacity of the soil is in defining the extent of the rooting depth. GLEAM takes into account 2.5m of the sub-surface linked to observed precipitation. On the other hand, transpiration in FLEX-Topo and WaPOR (ETLook model) is coupled to soil moisture in the root zone using an integrated approach. Consequently, this may explain why the pairwise comparison showed that trends and magnitudes of FLEX-Topo and WaPOR were not significantly ($p\text{-}value > 0.05$) different (in both dry miombo

woodland and wet miombo woodland) during the dormant phenophase (Tables A3, A4d in the supplementary data). Therefore, the integration of soil moisture in evaporation simulation and the accuracy of the soil moisture product used is likely to affect the accuracy of satellite-based transpiration estimates.

3.5.2 Optimisation of the rooting depth

Optimising rooting depth rather than the use of a standard depth has been shown to increase transpiration of trees in landscapes with a dry season (Kleidon and Heimann, 1998). Modifying rooting depth can improve energy flux simulations at both field scale and regional scale (Liu *et al.,* 2020). Wang-Erlandsson *et al.* (2016) showed that accurate root zone storage estimates "improved evaporation simulation overall, and in particular during the least evaporating months in sub-humid to humid regions with moderate to high seasonality". Their study demonstrated that several forest types have developed rootzone storage mechanisms that help buffering for dry season conditions. Some miombo species are deep rooting, beyond 5 metres, while the soil moisture in the miombo woodland increases with depth (i.e., Chidumayo, 2001; Savory, 1963). Therefore, one of the potential causes of the observed differences in satellite-based evaporation estimates could be the rooting depth used in the simulation of evaporation. The satellite-based evaporation estimates used in this study are likely not to have optimised rooting depth for the miombo woodland as there are few studies in the public domain that have investigated the optimum rooting depth for effective simulation of transpiration of miombo woodland. Since ecosystems have adapted to local climatic conditions (Tian *et al.,* 2018), global scale root storage estimates and optimisation may not be able to effectively capture the climatic conditions at local and region scales.

3.5.3 Differences in landcover products used

The landcover proxies in satellite-based evaporation estimates may also explain the observed differences in both temporal and spatial distribution of evaporation. For instance, the MOD16 uses a global landcover product (Gray *et al*., 2019; Running *et al*., 2019) which had shown to misclassify certain land cover types and showed low user accuracy in certain regions (i.e., Leroux *et al.,* 2014). WaPOR uses the Copernicus land cover product, but adds the distinction between irrigated and rain-fed areas (FAO, 2018). For the vegetation fraction, GLEAM uses MODIS MOD44B (Martens *et al.,* 2017; Miralles *et al.,* 2011). Other satellite-based evaporation estimates (i.e., SSEBop) use vegetation indices such as the NDVI as proxy for vegetation cover.

Different vegetation types have different phenology-water interactions (i.e., Lu *et al*., 2006) which influence actual evaporation (Forster *et al*., 2022; Snyder *et al*., 2013; Schwartz, 2013). Transpiration of the miombo woodland in the dry season is dependent on the landcover type and constrained by: root zone water availability (Wang-Erlandsson *et al.*, 2016; Gates & Hanks, 2015; Stancalie & Nert, 2012; Allen *et al.,* 1998), stomatal conductance thresholds and surface roughness, which are vegetation type and plant species dependent (i.e., Urban *et al.,* 2017; Wehr *et al.*, 2017; Gates & Hanks, 2015; Tuzet, 2011). Therefore, dissimilarities in the land cover products and their associated limitations possibly reflect in differences in the spatial-temporal distribution of satellite-based evaporation estimates.

3.5.4 Satellite-based rainfall products and rainfall interception

The differences observed in evaporation estimates may be related to differences in the quality of satellite-based precipitation products used and the ability of the models to effectively account for rainfall interception. Studies have shown that satellite precipitation products are

geographically biased towards either underestimation or overestimation (i.e., Macharia *et al.*, 2022; Asadullah *et al.*, 2008; Dinku *et al.*, 2007). In the case of Africa, and southern Africa in particular, no single precipitation product has been found to perform better than other precipitation products across landscapes (i.e., Macharia *et al.*, 2022). The difference in precipitation products, with different spatial resolutions and accuracy levels, may explain the differences in the spatial-temporal distribution of satellite-based evaporation estimates during the rainy season. For instance, FLEX-Topo used the Climate Hazards Group Infra-Red Precipitation with Station data (CHIRPS) (Funk *et al.*, 2015), GLEAM used Multi-Source Weighted-Ensemble Precipitation (MSWEP) (Bai and Liu, 2018), which uses different algorithms, inputs and spatial resolution.

Rainfall interception is a function of vegetation cover, leaf area (LAI), spatial scale and precipitation. For instance, LAI influences canopy interception, throughfall and forest floor interception, and spatial and temporal scale influences the interception threshold (FAO, 2018; Gerrits, 2010; Savenije, 2004). Field observations showed that wet miombo woodland canopies intercepted up to 18-20 percent of rainfall annually (i.e., Alexandre, 1977). Therefore, differences in the quality and accuracy of land cover products, and even proxies such as the NDVI used for modelling interception, are likely to result in different evaporation estimates of evaporation products that have interception modules (i.e., FLEX-Topo, GLEAM, MOD16 and WaPOR).

4 Conclusions and recommendations

The study sought to find out to which extent a variety of satellite-based evaporation estimates were in agreement or differed in quantifying miombo woodland evaporation during its typical phenophases and to establish the underlying factor(s) for the discrepancies that emerged. The study also compared the different evaporation estimates to the annual water balance-based evaporation at basin scale. The following were the conclusions:

Non-stationary time series showed strong similarity in temporal trends between satellite-based evaporation estimates and the changes in phenology (proxied by the LAI and NDVI) in the green-up and senescence/green-down phenophases. Weaker correlations in temporal trends of satellite-based evaporation estimates and changes in phenology where observed in the dormant phenophase and the maturity/peak phenophase.

Seasonally adjusted times series did not show strong similarity in temporal trends between satellite-based evaporation estimates and the changes in phenology, though the WaPOR showed relatively higher negative correlation values with the NDVI and LAI in the senescence/green-down phenophase and dormant phenophase in the dry season.

Both non-station time series and seasonally adjusted time series appeared to show weaker correlation and high coefficients of variation among satellite-based evaporation estimates in the dry season. The observed differences in satellite-based evaporation estimates in the dry season appear to be due to limited understanding and inadequate representation of the phenology-water interactions, that are influenced by the adapted physiological attributes such as the deep rooting and vegetation water storage of the miombo species.

It is possible that the underestimations of satellite-based evaporation estimates, compared to the water-balance based evaporation estimates, are affected by the disregard of over year storage in the deeper groundwater and the export of groundwater by leakage to the downstream Zambezi River. Another cause for the discrepancy is the inadequate representation of the phenology-water interactions of the miombo species, but also of other vegetation types such as the mopane woodland. Consequently, field observations of evaporation across the different phenophases and

strata of the miombo woodland are required to obtain a comprehensive overview of the characteristics of the actual evaporation of the ecosystem. This information can be used to help improve satellite-based evaporation assessments in the Luangwa Basin and the miombo region as whole.

Finally, in view of the unique phenology, whereby evaporation starts before the onset of rainfall, and the ability of the miombo species to access additional moisture stocks, inclusion of these traits is likely to improve estimates of transpiration of the miombo woodland in the dry season.

Author contribution

Conceptualization, H.Z.; formal analysis, H.Z., P.H; resources, H.S.; supervision, M.C.-G. and B.K.; writing—original draft, H.Z.; writing—review and editing, M.C.-G., B.K., H.S., P.H., I.N., and N.V. All authors have read and agree to the published version of the manuscript.

Funding

This study was conducted with the financial support of the Dutch Research Council (NWO) under the project number W 07.303.102.

Acknowledgements

This study is part of the ZAMSECUR Project, which focuses on observing and understanding the remote water resources for enhancing water, food and energy security in Lower Zambezi Basin We wish to thank the Water Resources Management Authority (WARMA) in Zambia for the field discharge data used in this study.

Conflict of interest:

At least one of the (co-)authors is a member of the editorial board of Hydrology and Earth System Sciences.

References

Abatzoglou, J. T., Dobrowski, S. Z., Parks, S. A., & Hegewisch, K. C.: TerraClimate, a high-resolution global dataset of monthly climate and climatic water balance from 1958-2015. *Scientific Data*, *5*, 1–12. doi:10.1038/sdata.2017.191, 2018.

Abrams, M., & Crippen, R.: ASTER Global DEM (Digital Elevation Mode) - Quick Guide for V3. *California Institute of Technology*, *3*(July), 10, 2019.

Allen R., G., Pereira L. S., Raes D, Smith M.: Crop evapotranspiration - guidelines for computing crop water requirements. FAO irrigation and drainage paper 56, Rome, Italy http://www.fao.org/docrep/X0490E/X0490E00.htm, 1998.

Alexandre, J.: Le bilan de l'eau dans le miombo (forêt claire tropicale). Bulletein de la Société Géographie du Liège 13, 107-126, 1977.

Asadullah, A., McIntyre, N., & Kigobe, M.: Evaluation of five satellite products for estimation of rainfall over Uganda. *Hydrological Sciences Journal*, *53*(6), 1137–1150. doi:10.1623/hysj.53.6.1137, 2008.

Bai, P. and Liu, X.: Intercomparison and evaluation of three global high-resolution evapotranspiration products across China, J. Hydrol., 566, 743–755, https://doi.org/10.1016/j.jhydrol.2018.09.065, 2018.

Beilfuss, R.: A Risky Climate for Southern African Hydro ASSESSING HYDROLOGICAL RISKS AND A Risky Climate for Southern African Hydro, (September). doi:10.13140/RG.2.2.30193.48486, 2012.

Biggs, T., Petropoulos, G. P., Velpuri, N. M., Marshall, M., Glenn, E. P., Nagler, P., & Messina, A.: Remote sensing of actual evapotranspiration from croplands. Remote Sensing Handbook: Remote Sensing of Water Resources, Disasters, and Urban Studies, 59-99, 2015.

Bogawski, P., Bednorz, E.: Comparison and Validation of Selected Evapotranspiration Models for Conditions in Poland (Central Europe). *Water Resour Manage* **28**, 5021–5038. https://doi.org/10.1007/s11269-014-0787-8, 2014.

Bonnesoeur, V., Locatelli, B., Guariguata, M. R., Ochoa-Tocachi, B. F., Vanacker, V., Mao, Z., … Mathez-Stiefel, S. L.: Impacts of forests and forestation on hydrological services in the Andes: A systematic review. *Forest Ecology and Management*, *433*(June 2018), 569–584. doi:10.1016/j.foreco.2018.11.033, 2019.

Brust, C., Kimball, J. S., Maneta, M. P., Jencso, K., He, M., & Reichle, R. H.: Using SMAP Level-4 soil moisture to constrain MOD16 evapotranspiration over the contiguous USA. *Remote Sensing of Environment*, *255*(January), 112277. doi:10.1016/j.rse.2020.112277, 2021.

Briuinger, D R, P R Krishnaiah, and William S Cleveland. “Seasonal and Calendar Adjustment.” *Handbook of Statistics* 3: 39–72, 1983.

Buchhorn, M.; Smets, B.; Bertels, L.; De Roo, B.; Lesiv, M.; Tsendbazar, N.E., Linlin, L., Tarko, A.: *Copernicus Global Land Service: Land Cover 100m: Version 3 Globe 2015-2019: Product User Manual*. Zenodo, Geneve, Switzerland. https://doi.org/10.5281/zenodo.3938963, 2020.

Campbell, B., Frost, P., & Bryon, N.: miombo woodlands and their use: overview and key issues.In “The Miombo in Transition: Woodlands and Welfare in Africa. Ed: B. Campbell (Bogor, Indonesia: Center for International Forestry Research) p 1–6, 1996.

Chen, Y., Xia, J., Liang, S., Feng, J., Fisher, J. B., Li, X., … Yuan, W.: Comparison of satellite-based evapotranspiration models over terrestrial ecosystems in China. *Remote Sensing of Environment*, *140*, 279–293. doi:10.1016/j.rse.2013.08.045, 2014.

Chidumayo, E. N.: Climate and Phenology of Savanna Vegetation in Southern Africa. *Journal of Vegetation Science*, *12*(3), 347. doi: 10.2307/3236848, 2001.

Chidumayo, E, N., & Frost, P.: Population biology of miombo trees. In The miombo in transition: woodlands and welfare in Africa, Campbell, B. (ed.). Bogor (Indonesia): CIFOR, ISBN 979-8764-07-2, 1996.

Chidumayo, E. N.: Phenology and nutrition of miombo woodland trees in Zambia. *Trees*, *9*(2), 67–72. doi:10.1007/BF00202124, 1994.

Cleland, E. E., Chuine, I., Menzel, A., Mooney, H. A., & Schwartz, M. D.: Shifting plant phenology in response to global change. *Trends in Ecology and Evolution*, *22*(7), 357–365. doi:10.1016/j.tree.2007.04.003, 2007.

Dinku, T., Ceccato, P., Grover-Kopec, E., Lemma, M., Connor, S. J., & Ropelewski, C. F.: Validation of satellite rainfall products over East Africa's complex topography. *International Journal of Remote Sensing*, *28*(7), 1503–1526. doi:10.1080/01431160600954688, 2007.

Ernst, W. and Walker, B.H.: Studies on the hydrature of trees in miombo woodland in South Central Africa. Journal of Ecology 61, 667-673, 1973.

FAO.: *WaPOR Database Methodology: Level 1 Data*. *Remote Sensing for Water Productivity Technical Report: Methodology Series.* Retrieved from http://www.fao.org/fileadmin/user_upload/faoweb/RS-WP/pdf_files/Web_WaPOR-beta_Methodology_document_Level1.pdf, last accessed: 20 June, 2022, 2018

Forrest, J., Inouye, D. W., & Thomson, J. D.: Flowering phenology in subalpine meadows: Does climate variation influence community co-flowering patterns? *Ecology*, *91*(2), 431–440. doi:10.1890/09-0099.1, 2010.

Forrest, J., & Miller-Rushing, A. J.: Toward a synthetic understanding of the role of phenology in ecology and evolution. *Philosophical Transactions of the Royal Society B: Biological Sciences*, *365*(1555), 3101–3112. doi:10.1098/rstb.2010.0145, 2010.

Forster, M. A., Kim, T. D. H., Kunz, S., Abuseif, M., Chulliparambil, V. R., Srichandra, J., & Michael, R. N.: Phenology and canopy conductance limit the accuracy of 20 evapotranspiration models in predicting transpiration. *Agricultural and Forest Meteorology*, *315*(December 2021), 108824. doi:10.1016/j.agrformet.2022.108824, 2022.

Friedl, M., Gray, J., Sulla-Menashe, D.: MCD12Q2 MODIS/Terra+Aqua Land Cover Dynamics Yearly L3 Global 500m SIN Grid V006 [Data set]. NASA EOSDIS Land Processes DAAC. Accessed 2023-03-30 from https://doi.org/10.5067/MODIS/MCD12Q2.006, 2019.

Frost, P.: *The Ecology of Miombo Woodlands*. (B. Campbell, Ed.), *The Miombo in Transition: Woodlands and Welfare in Africa*. Bogor, Indonesia: Center for International Forestry Research. Retrieved from http://books.google.com/books?hl=nl&lr=&id=rpildJJVdU4C&pgis=1, last accessed: 20 June 2022, 1996.

Fuller, D. O.: Canopy phenology of some mopane and miombo woodlands in eastern Zambia. *Global Ecology and Biogeography*, *8*(3–4), 199–209. doi:10.1046/j.1365-2699.1999.00130.x, 1999.

Fuller, D. O., & Prince, S. D.: Rainfall and foliar dynamics in tropical southern Africa: Potential impacts of global climatic change on Savanna vegetation. *Climatic Change*, *33*(1), 69–96. doi:10.1007/BF00140514, 1996.

Funk, C., Peterson, P., Landsfeld, M., Pedreros, D., Verdin, J., Shukla, S., Husak, G., Rowland, J., Harrison, L., Hoell, A., & Michaelsen, J.: The climate hazards infrared precipitation with stations - A new environmental record for monitoring extremes. *Scientific Data*, *2*, 1–21. doi: 10.1038/sdata.2015.66, 2015.

García, L., Rodríguez, J. D., Wijnen, M., & Pakulski, I.: *Earth Observation for Water Resources Management: Current Use and Future Opportunities for the Water Sector*. Washington, DC 20433: Washington, DC: World Bank. doi:10.1596/978-1-4648-0475-5, 2016.

Gates, D. M., & Hanks, R. J.: Plant factors affecting evapotranspiration. *Irrigation of Agricultural Lands*, *11*, 506–521. doi:10.2134/agronmonogr11.c28, 2015.

Gerrits, A.M.J.: The role of interception in the hydrological cycle. Dissertation Delft University of Technology. ISBN: 978-90-6562-248-8 http://resolver.tudelft.nl/uuid:7dd2523b-2169-4e7e-992c-365d2294d02e, 2010.

Ghysels, Eric, Denise R. Osborn, and Paulo M.M. Rodrigues. "Chapter 13 Forecasting Seasonal Time Series." *Handbook of Economic Forecasting*. https://doi.org/10.1016/S1574-0706(05)01013-X, 2006.

Gokmen, M., Vekerdy, Z., Verhoef, A., Verhoef, W., Batelaan, O., & van der Tol, C.: Integration of soil moisture in SEBS for improving evapotranspiration estimation under water stress conditions. *Remote Sensing of Environment*, *121*, 261–274. doi:10.1016/j.rse.2012.02.003, 2012.

Gray, J., Sulla-Menashe, D., & Friedl, M. A: MODIS Land Cover Dynamics (MCD12Q2) Product. *User Guide Collection 6*, *6*, 8. Retrieved from https://modis-land.gsfc.nasa.gov/pdf/MCD12Q2_Collection6_UserGuide.pdf, last accessed: 20 June 2022, 2019.

Guan, K., Eric F. Wood, D. Medvigy, John. Kimball, Ming. Pan, K.K. Caylor, J. Sheffield, Xiangtao. Xu, and O.M. Jones.: Terrestrial hydrological controls on land surface phenology of African savannas and woodlands. *Journal of Geophysical Research: Biogeosciences*, *119*(8), 1652–1669. doi:10.1002/2013JG002572, 2014, 2014.

Han, J., Zhao, Y., Wang, J., Zhang, B., Zhu, Y., Jiang, S., & Wang, L.: Effects of different land use types on potential evapotranspiration in the Beijing-Tianjin-Hebei region, North China. *Journal of Geographical Sciences*, *29*(6), 922–934. doi:10.1007/s11442-019-1637-7, 2019.

Helsel, D. R., R. M. Hirsch, K.R. Ryberg, S.A. Archfield, and E.J. Gilroy.: "Statistical Methods in Water Resources Techniques and Methods 4 – A3." *USGS Techniques and Methods*, 2020.

Hersbach, H., Bell, B., Berrisford, P., Hirahara, S., Horányi, A., Muñoz-Sabater, J., Nicolas, J., Peubey, C., Radu, R., Schepers, D., Simmons, A., Soci, C., Abdalla, S., Abellan, X., Balsamo, G., Bechtold, P., Biavati, G., Bidlot, J., Bonavita, M., De Chiara, G., Dahlgren, P., Dee, D., Diamantakis, M., Dragani, R., Flemming, J., Forbes, R., Fuentes, M., Geer, A., Haimberger, L., Healy, S., Hogan, R.J., Hólm, E., Janisková, M., Keeley, S., Laloyaux, P., Lopez, P., Lupu, C., Radnoti, G., de Rosnay, P., Rozum, I., Vamborg, F., Villaume, S., Thépaut, J-N.: Complete ERA5 from 1979: Fifth generation of ECMWF atmospheric reanalyses of the global climate. Copernicus Climate Change Service (C3S) Data Store (CDS). (Accessed on 06-06-2022), 2017.

Hulsman, P., Hrachowitz, M., & Savenije, H. H. G.: Improving the Representation of Long-Term Storage Variations With Conceptual Hydrological Models in Data-Scarce Regions. *Water Resources Research*, *57*(4). doi:10.1029/2020WR028837, 2021.

Hulsman, P., Winsemius, H. C., Michailovsky, C. I., Savenije, H. H. G., & Hrachowitz, M.: Using altimetry observations combined with GRACE to select parameter sets of a hydrological model in a data-scarce region. *Hydrology and Earth System Sciences*, *24*(6), 3331–3359. doi:10.5194/hess-24-3331-2020, 2020.

Jeffers, J. N., & Boaler, S. B., 1966. Ecology of a miombo site. Lupa North Forest Reserve, Tanzania. I. Weather and plant growth , 1962–64'. *Ecology*, *54*, 447–463.

Jiménez, C., Prigent, C., Mueller, B., Seneviratne, S. I., McCabe, M. F., Wood, E. F., … Wang, K.: Global intercomparison of 12 land surface heat flux estimates. *Journal of Geophysical Research Atmospheres*, *116*(2), 1–27. doi:10.1029/2010JD014545, 2011.

Jiménez, C., Prigent, C., & Aires, F.: Toward an estimation of global land surface heat fluxes from multisatellite observations. *Journal of Geophysical Research Atmospheres*, *114*(6), 1–22. doi:10.1029/2008JD011392, 2009.

Kleine, L., Tetzlaff, D., Smith, A., Dubbert, M., & Soulsby, C.: Modelling ecohydrological feedbacks in forest and grassland plots under a prolonged drought anomaly in Central Europe 2018–2020. *Hydrological Processes*, *35*(8). doi:10.1002/hyp.14325, 2021.

Kramer, K., Leinonen, I., & Loustau, D.: The importance of phenology for the evaluation of impact of climate change on growth of boreal, temperate and Mediterranean forests ecosystems: An overview. *International Journal of Biometeorology*. doi:10.1007/s004840000066, 2000.

Leroux, L., Jolivot,A., Bégué,A., Lo Seen,D., and Zoungrana, B.: "How Reliable Is the MODIS Land Cover Product for Crop Mapping Sub-Saharan Agricultural Landscapes?" *Remote Sensing* 6(9):8541–64. doi: 10.3390/rs6098541, 2014.

Li, H., Ma, X., Lu, Y., Ren, R., Cui, B., & Si, B.: Growing deep roots has opposing impacts on the transpiration of apple trees planted in subhumid loess region. Agricultural Water Management, 258(June), 107207. doi: 10.1016/j.agwat.2021.107207, 2021.

Liu. M, & Hu. D.: Response of Wetland Evapotranspiration to Land Use/Cover Change and Climate Change in Liaohe River Delta, China. *Water*; 11(5):955. https://doi.org/10.3390/w11050955, 2019.

Liu, Wenbin, Lei Wang, Jing Zhou, Yanzhong Li, Fubao Sun, Guobin Fu, Xiuping Li, and Yan Fang Sang.: "A Worldwide Evaluation of Basin-Scale Evapotranspiration Estimates against the Water Balance Method." *Journal of Hydrology* 538: 82–95. https://doi.org/10.1016/j.jhydrol.2016.04.006, 2016.

Lu, P., Yu, Q., Liu, J., & Lee, X.: Advance of tree-flowering dates in response to urban climate change. *Agricultural and Forest Meteorology*, *138*(1–4), 120–131. doi:10.1016/j.agrformet.2006.04.002, 2006.

Macharia, D., Fankhauser, K., Selker, J. S., Neff, J. C., & Thomas, E. A.: Validation and Intercomparison of Satellite-Based Rainfall Products over Africa with TAHMO In Situ Rainfall Observations. *Journal of Hydrometeorology*, *23*(7), 1131–1154. doi:10.1175/JHM-D-21-0161.1, 2022.

Makapela, L.: *Review and use of earth observations and remote sensing in water resource management in South Africa : report to the Water Research Commission*, 2015.

Marchesini, V. A., Fernández, R. J., Reynolds, J. F., Sobrino, J. A., & Di Bella, C. M.: Changes in evapotranspiration and phenology as consequences of shrub removal in dry forests of central Argentina. *Ecohydrology*, *8*(7), 1304–1311. doi:10.1002/eco.1583, 2015.

Martens, B., Miralles, D. G., Lievens, H., Van Der Schalie, R., De Jeu, R. A. M., Fernández-Prieto, D., … Verhoest, N. E. C.: GLEAM v3: Satellite-based land evaporation and root-zone soil moisture. *Geoscientific Model Development*, *10*(5), 1903–1925. doi:10.5194/gmd-10-1903-2017, 2017.

Martins, J. P., Trigo, I., & Freitas, S. C. E.: Copernicus Global Land Operations "Vegetation and Energy" "CGLOPS-1". *Copernicus Global Land Operations*, 1–93. doi:10.5281/zenodo.3938963.PU, 2020.

Miralles, D. G., Brutsaert, W., Dolman, A. J., & Gash, J. H.: On the Use of the Term "Evapotranspiration". *Water Resources Research*, *56*(11). doi:10.1029/2020WR028055, 2020.

Miralles, D. G., De Jeu, R. A. M., Gash, J. H., Holmes, T. R. H., & Dolman, A. J.: Magnitude and variability of land evaporation and its components at the global scale. *Hydrology and Earth System Sciences*, *15*(3), 967–981. doi:10.5194/hess-15-967-2011, 2011.

Mittermeier, R. A., Mittermeier, C. G., Brooks, T. M., Pilgrim, J. D., Konstant, W. R., Da Fonseca, G. A. B., & Kormos, C.: Wilderness and biodiversity conservation. *Proceedings of the National Academy of Sciences of the United States of America*, *100*(18), 10309–10313. doi:10.1073/pnas.1732458100, 2003.

Mu, Q., Zhao, M., and Running, W.S.: Improvements to a MODIS Global Terrestrial Evapotranspiration Algorithm. *Remote Sensing of Environment* 115 (8): 1781–1800. https://doi.org/10.1016/j.rse.2011.02.019, 2011.

Mu, Q., Heinsch, F. A., Zhao, M., & Running, S. W.: Development of a global evapotranspiration algorithm based on MODIS and global meteorology data. *Remote Sensing of Environment*, *111*(4), 519–536. doi:10.1016/j.rse.2007.04.015, 2007.

Myneni, R., Knyazikhin, Y., and Park, T.: MCD15A2H MODIS/TerraCAqua Leaf Area Index/FPAR 8-day L4 Global 500m SIN Grid V06, NASA EOSDIS Land Processes DAAC [data set], https://doi.org/10.5067/MODIS/MCD15A2H.061, 2021.

Myneni, R., & Park, Y. K.: *MCD15A2H MODIS/Terra+Aqua Leaf Area Index/FPAR 8-day L4 Global 500m SIN Grid V006.* NASA EOSDIS Land Processes DAAC. Retrieved from https://doi.org/10.5067/MODIS/MCD15A2H.006, (last accessed: 20 January, 2023) 2015.

Nelson, Michael, Tim Hill, William Remus, and Marcus O'connor. "Time Series Forecasting Using Neural Networks: Should the Data Be Deseasonalized First?" *Journal of Forecasting* 18: 359–67, 1999.

Niu,S., Fu,Y., Gu,L., and and Luo, Y.: Temperature Sensitivity of Canopy Photosynthesis Phenology in Northern Ecosystems. Pp. 503–19 in *Phenology: An Integrative Environmental Science*, edited by M. D. Schwartz., 2013.

Nord, E. A., & Lynch, J. P.: Plant phenology: A critical controller of soil resource acquisition. *Journal of Experimental Botany*, *60*(7), 1927–1937. doi:10.1093/jxb/erp018, 2009.

Novick, K. A., Ficklin, D. L., Stoy, P. C., Williams, C. A., Bohrer, G., Oishi, A. C., Papuga, S. A., Blanken, P. D., Noormets, A., Sulman, B. N., Scott, R. L., Wang, L., & Phillips, R. P.: The increasing importance of atmospheric demand for ecosystem water and carbon fluxes. *Nature Climate Change*, *6*(11), 1023–1027. doi:10.1038/nclimate3114, 2016.

ORNL DAAC., 2018. MODIS and VIIRS Land Products Global Subsetting and Visualization Tool, Subset obtained for MCD12Q2 product at [-12:76252], [32.48406], time period: [31-12-2020] to [31-12-2021], and subset size: [4]_[4] km,ORNL DAAC, Oak Ridge, Tennessee, USA [data set],https://doi.org/10.3334/ORNLDAAC/1379.

Pelletier, J., Paquette, A., Mbindo, K., Zimba, N., Siampale, A., Chendauka, B., Siangulube, F., & Roberts, J. W.: Carbon sink despite large deforestation in African tropical dry forests (miombo woodlands). *Environmental Research Letters*, *13*(9). doi:10.1088/1748-9326/aadc9a, 2018.

Pereira, C. C., Boaventura, M. G., Cornelissen, T., Nunes, Y. R. F., & de Castro, G. C.: What triggers phenological events in plants under seasonal environments? A study with phylogenetically related plant species in sympatry. *Brazilian Journal of Biology*, *84*(March). doi:10.1590/1519-6984.257969, 2022.

Roberts, J. M.: *The role of forests in the hydrological cycle*. *Forests and forest plants* (Vol. III). Retrieved from https://www.eolss.net/sample-chapters/c10/E5-03-04-02.pdf, last accessed: 20 June, 2022, (not dated).

Running, Steven W, Qiaozhen Mu, Maosheng Zhao, A. M.:. User ' s Guide MODIS Global Terrestrial Evapotranspiration (ET) Product NASA Earth Observing System MODIS Land Algorithm (For Collection 6) (last accessed: 20 January, 2023), 2019.

Ryan, C. M., Pritchard, R., McNicol, I., Owen, M., Fisher, J. A., & Lehmann, C.: Ecosystem services from southern African woodlands and their future under global change.

Philosophical Transactions of the Royal Society B: Biological Sciences, *371*(1703). doi:10.1098/rstb.2015.0312, 2016.

Saha, S., Moorthi, S., Wu, X., Wang, J., & Coauthors.: The NCEP Climate Forecast System Version 2. *Journal of Climate, 27*, 2185–2208. doi:10.1175/JCLI-D-12-00823.1, 2014.

Saha, S., Moorthi, S., Pan, H., Wu,, X., Wang, J., & Coauthors.: The NCEP Climate Forecast System Reanalysis. *Bulletin of the American Meteorological Society, 91*, 1015–1057. doi:10.1175/2010BAMS3001.1, 2010.

Santin-Janin, H., Garel, M., Chapuis, J. L., & Pontier, D.: Assessing the performance of NDVI as a proxy for plant biomass using non-linear models: A case study on the kerguelen archipelago. *Polar Biology*, *32*(6), 861–871. doi:10.1007/s00300-009-0586-5, 2009.

Savenije, H. H.G.: HESS opinions 'topography driven conceptual modelling (FLEX-Topo)'. *Hydrology and Earth System Sciences*, *14*(12), 2681–2692. doi:10.5194/hess-14-2681-2010, 2010.

Savenije, Hubert H.G.: The importance of interception and why we should delete the term evapotranspiration from our vocabulary. *Hydrological Processes*, *18*(8), 1507–1511. doi:10.1002/hyp.5563, 2004.

Savory, B. M.: Site quality and tree root morphology in Northern Rhodesia, Rhodes. J. Agricult. Res., 1, 55–64, 1963.

Schwartz, M. D.: *Phenology: An Integrative Environmental Science*. (M. D. Schwartz, Ed.), *Phenology: An Integrative Environmental Science* (Second Edi). Dordrecht: Springer Netherlands. doi:10.1007/978-94-007-6925-0_27, 2013.

Senay, G. B., Bohms, S., Singh, R. K., Gowda, P. H., Velpuri, N. M., Alemu, H., & Verdin, J. P.: Operational Evapotranspiration Mapping Using Remote Sensing and Weather Datasets: A New Parameterization for the SSEB Approach. *Journal of the American Water Resources Association*, *49*(3), 577–591. doi:10.1111/jawr.12057, 2013.

Shahidan, M. F., Salleh, E., & Mustafa, K. M. S.: Effects of tree canopies on solar radiation filtration in a tropical microclimatic environment. *Sun, Wind and Architecture - The Proceedings of the 24th International Conference on Passive and Low Energy Architecture, PLEA 2007*, (November), 400–406, 2007.

Sheil, D.: Forests, atmospheric water and an uncertain future: the new biology of the global water cycle. *Forest Ecosystems*, *5*(1). doi:10.1186/s40663-018-0138-y, 2018.

Snyder, R. L., & Spano, D.: Phenology and Evapotranspiration. In Mark D. Schwartz (Ed.), *Phenology: An Integrative Environmental Science* (Second, pp. 521–528). Milwaukee, 2013.

Stancalie, G., & Nert, A.: Possibilities of Deriving Crop Evapotranspiration from Satellite Data with the Integration with Other Sources of Information. *Evapotranspiration - Remote Sensing and Modeling*, (January). doi:10.5772/23635, 2012.

Stökli, R., T. Rutishauser, I. Baker, M. A. Liniger, and A. S. Denning.: “A Global Reanalysis of Vegetation Phenology.” *Journal of Geophysical Research: Biogeosciences* 116 (3): 1–19. https://doi.org/10.1029/2010JG001545, 2011.

Tian, F., Wigneron, J. P., Ciais, P., Chave, J., Ogée, J., Peñuelas, J., … Fensholt, R.: Coupling of ecosystem-scale plant water storage and leaf phenology observed by satellite. *Nature Ecology and Evolution*, *2*(9), 1428–1435. doi:10.1038/s41559-018-0630-3, 2018.

Tuzet, A. J.: Stomatal Conductance, Photosynthesis, and Transpiration, Modeling. In J. Gliński, J., Horabik, J., Lipiec (Ed.), *Encyclopedia of Agrophysics. Encyclopedia of Earth Sciences Series* (pp. 855–858). Dordrecht. doi:10.1007/978-90-481-3585-1_213, 2011.

Urban, J., Ingwers, M. W., McGuire, M. A., & Teskey, R. O.: Increase in leaf temperature opens stomata and decouples net photosynthesis from stomatal conductance in Pinus taeda and Populus deltoides x nigra. *Journal of Experimental Botany*, *68*(7), 1757–1767. doi:10.1093/jxb/erx052, 2017.

Van Der Ent, R. J., Wang-Erlandsson, L., Keys, P. W., & Savenije, H. H. G.: Contrasting roles of interception and transpiration in the hydrological cycle – Part 2: Moisture recycling. *Earth System Dynamics*, *5*(2), 471–489. doi:10.5194/esd-5-471-2014, 2014.

Van Der Ent, Rudi J., Savenije, H. H. G., Schaefli, B., & Steele-Dunne, S. C.: Origin and fate of atmospheric moisture over continents. *Water Resources Research*, *46*(9), 1–12. doi:10.1029/2010WR009127, 2010

Vermote, E., Wolfe, R.: MOD09GA MODIS/Terra Surface Reflectance Daily L2G Global 1kmand 500m SIN Grid V006 [Data set]. NASA EOSDIS Land Processes DAAC. Accessed 2022-10-01 from https://doi.org/10.5067/MODIS/MOD09GA.006, 2015.

Vinya, R., Malhi, Y., Brown, N. D., Fisher, J. B., Brodribb, T., & Aragão, L. E.: Seasonal changes in plant–water relations influence trends of leaf display in Miombo woodlands: evidence of water conservative strategies. *Tree Physiology, 39,* 04–112. doi:doi:10.1093/treephys/tpy062, 2018.

Wang, S., Fu, B. J., Gao, G. Y., Yao, X. L., & Zhou, J.: Soil moisture and evapotranspiration of different land cover types in the Loess Plateau, China. *Hydrology and Earth System Sciences*, *16*(8), 2883–2892. doi: 10.5194/hess-16-2883-2012, 2012.

Wang-Erlandsson, L., Bastiaanssen, W. G. M., Gao, H., Jägermeyr, J., Senay, G. B., Van Dijk, A. I. J. M., … Savenije, H. H. G.: Global root zone storage capacity from satellite-based evaporation. *Hydrology and Earth System Sciences*, *20*(4), 1459–1481. doi:10.5194/hess-20-1459-2016, 2016.

WARMA.: Catchments for Zambia. Retrieved 9 February 2022, from http://www.warma.org.zm/catchments-zambia/luangwa-catchment-2/, 2022.

Weerasinghe, I., Bastiaanssen, W., Mul, M., Jia, L., & Van Griensven, A.: Can we trust remote sensing evapotranspiration products over Africa. *Hydrology and Earth System Sciences*, *24*(3), 1565–1586. doi:10.5194/hess-24-1565-2020, 2020.

Wehr, R., Commane, R., Munger, J. W., Barry Mcmanus, J., Nelson, D. D., Zahniser, M. S., … Wofsy, S. C.: Dynamics of canopy stomatal conductance, transpiration, and evaporation in a temperate deciduous forest, validated by carbonyl sulfide uptake. *Biogeosciences*, *14*(2), 389–401. doi:10.5194/bg-14-389-2017, 2017.

White, F.: *The Vegetation of Africa; a descriptive memoir to accompany the UNESCO/AETFAT/UNSO vegetation map of Africa*. Paris: UNESCO. Retrieved from https://unesdoc.unesco.org/ark:/48223/pf0000058054 (Last accessed: 20 January, 2023), 1983.

World Bank.: "The Zambezi River Basin: A Multi-Sector Investment Opportunities Analysis – State of the Basin," World Bank Publications - Reports 2961, The World Bank Group. https://ideas.repec.org/p/wbk/wboper/2961.html, (Last accessed: 20 January 2023), 2010.

Zhang, K, Kimball, S. J., and Running, W.S.: A Review of Remote Sensing Based Actual Evapotranspiration Estimation. *Wiley Interdisciplinary Reviews: Water* 3 (6): 834–53. https://doi.org/10.1002/wat2.1168, 2016.

Zhang, X., Friedl, M. A., Schaaf, C. B., Strahler, A. H., Hodges, J. C. F., Gao, F., Reed, B. C., & Huete, A.: Monitoring vegetation phenology using MODIS. *Remote Sensing of Environment*, *84*(3), 471–475. doi: 10.1016/S0034-4257(02)00135-9, 2003.

Zhao, M, Peng, C., Xiang, W., Deng, X., Tian, D., Zhou, X., Yu, G., He, H., and Zhao, Z.: "Plant Phenological Modeling and Its Application in Global Climate Change Research: Overview and Future Challenges." *Environmental Reviews* 21 (1): 1–14. https://doi.org/10.1139/er-2012-0036, 2013

Zimba, H., Coenders-Gerrits, M., Banda, K., Schilperoort, B., van de Giesen, N., Nyambe, I., and Savenije, H. H. G.: Phenophase-based comparison of field observations to satellite-based actual evaporation estimates of a natural woodland: miombo woodland, southern Africa, Hydrol. Earth Syst. Sci., 27, 1695–1722, https://doi.org/10.5194/hess-27-1695-2023, 2023.

Zimba, H., Coenders, M., Savenije, H. H. G., van de Giesen, N., & Hulsman, P.: ZAMSECUR Project Field Data Mpika, Zambia (Version 2) [Data set]. 4TU.ResearchData. https://doi.org/10.4121/19372352.V2, 2022.